The application of an implicit TVD method for water flow modelling in channels and pipes.[1]

P. Garcia-Navarro[2] and A. Priestley

Dept. of Mathematics,

P.O. Box 220,

University of Reading,

Whiteknights,

Reading,

U.K.

Keywords: Implicit TVD methods, pressurised flows, flow in a pipe network.

[1]The first author was funded by the Spanish Ministerio de Educacion y Ciencia and the second by the U.K. Science and Engineering Research Council.

[2]On leave from the University of Zaragoza

Abstract

An implicit time integration method for the simulation of steady and unsteady flow in pipes and channels is presented. It is based on the theory of Total Variation Diminishing (TVD) methods. A conservative linearization leads to a block tridiagonal system of equations which can be cheaply solved by means of a non-iterative LU decomposition method. It keeps the advantages of classical implicit schemes, in the sense that the traditional CFL limit is removed, and properly deals with all kinds of flow. It is specially suited for steady flows including phenomena such as hydraulic jumps and also gives satisfactory results for time dependent problems. Several test cases are shown to illustrate the performance of this implicit technique in single channels. The applicability of this numerical scheme to the simulation of steady and transient flows in pipe networks is also demonstrated through some examples.

1 Introduction

Numerical methods to predict the water profile and discharge in steady as well as unsteady situations of hydraulic systems have become a common tool. Finite difference applications of numerical schemes in particular have been widely reported (see, for instance, Cunge et al. 1980).

One of the characteristics that renders explicit schemes attractive is their conceptual simplicity. Variables at a future time can be evaluated at every grid point through simple algebraic calculations involving already known values. On the other hand, the time step size is usually restricted by stability reasons, typically expressed as a limit on the CFL number that can be taken.

Another option is the choice of implicit schemes in which the variables must be calculated simultaneously, through the resolution of a system with as many unknowns as grid points, in the new time level. If the problem is nonlinear, so is the resulting system, and either a linearization or an iterative procedure is required. The extra work is usually compensated for by unconditional stability, allowing time steps as big as desired, or permitted, by the particular problem under consideration. They are the ideal candidates for the calculation of steady states but can also be efficient in the simulation of transients.

Difficult situations, in which mixed regimes with surface discontinuities are present, usually invalidate the classical methods, justifying the search for new techniques. The effort made in gas-dynamics to develop efficient Euler solvers led to a class of methods based on the Total Variation Diminishing (TVD) property (Sweby, 1984), characterised by their robustness and accuracy. This generation of techniques can also be cast as improved conservative second order classical schemes.

In this work, the performance of an implicit method based on a TVD theory when applied to the 1-D shallow water equations for the simulation

of free-surface as well as pressurised flows is investigated.

First, the equations we are going to solve are presented. They are essentially the well known Saint Venant equations written in conservative form. Some usual modifications intended to render them able to cope with pressurised flows whilst keeping their form are also included. Then, the implicit technique is introduced and applied to the system of equations. A conservative linearization is adapted to the basic method in order to simplify the resulting algebraic equations and be able to work out an algebraic block tridiagonal matrix system. The numerical treatment of external, as well as internal, boundary conditions is described.

A variety of hydraulic test cases is presented to assess the validity of the method. Then it is also successfully applied to the problem of flow simulation in a pipe system.

2 The equations

It is generally accepted that the unsteady flow of water, in a one-dimensional approach, is governed by the shallow water or St. Venant equations. These represent mass and momentum conservation along the direction of the main flow. It constitutes an adequate description for most of the problems associated with pipe flow modelling and can be written as the following system of equations:

$$\begin{aligned} &\frac{\partial A}{\partial t} + \frac{\partial Q}{\partial x} = 0 \\ &\frac{\partial Q}{\partial t} + \frac{\partial}{\partial x}\left(\frac{Q^2}{A} + gI_1\right) = gI_2 + gA(S_0 - S_f) \end{aligned} \tag{2.1}$$

where A is the wetted cross sectional area, Q is the discharge and g is the acceleration due to gravity. I_1 represents a hydrostatic pressure force term

$$I_1 = \int_0^{h(x,t)} (h - \eta) b(x, \eta) d\eta \tag{2.2}$$

with

$$b(x,\eta) = \frac{\partial A(x,\eta)}{\partial \eta}$$

and I_2 accounts for the pressure forces due to longitudinal width variations,

$$I_2 = \int_0^{h(x,t)} (h-\eta)\frac{\partial b(x,\eta)}{\partial x} d\eta.$$

The right hand side of equation (2.1) contains also the sources and sinks of momentum arising from the bed slope and the friction losses. The bed slope is the spatial partial derivative of the bottom elevation z,

$$S_0 = -\frac{\partial z}{\partial x}$$

and the friction slope is defined, in terms of the Manning's roughness coefficient n,

$$S_f = \frac{Q\,|Q|\,n^2}{A^2 R^{\frac{4}{3}}} \tag{2.3}$$

with $R = A/P$, P being the wetted perimeter. Other forms of S_f can equally well be used.

All the cases that we are going to deal with in this work involve prismatic channels, so that the I_2 pressure term will not be used. On the other hand, we will be interested in the transients from partially filled to full pipes, that is, the change from open channel to pressurised flow in closed channels. The usual way to automatically take this into account without changing the governing equations is well described in Baines et al., 1992, for example. It consists of assuming the presence of a very narrow and infinitely high slot all along the pipe. It will become filled by water in the event of pressurised flow, providing the extra hydrostatic pressure whilst still allowing the use of the open channel flow equations.

In the case of a rectangular pipe of constant width b_p and height h_p and a slot of width b_s, the following formulae are going to be used:

$\underline{A < A_p}$:

$$h = \frac{A}{b_p}$$

$$I_1 = \frac{A^2}{2b_p}$$

$$P = b_p + 2h$$

$\underline{A > A_p}$:

$$h = \frac{A - A_p}{b_s} + h_p$$

$$I_1 = A_p(\frac{A - A_p}{b_s} + \frac{h_p}{2}) + \frac{(A - A_p)^2}{2b_s}$$

$$P = 2b_p + 2h_p$$

where $A_p = b_p h_p$. At the same time the wave celerity, c, defined as:

$$c^2 = \frac{\partial I_1}{\partial A}$$

changes from $c = \sqrt{gA/b_p}$ to $c = \sqrt{gA/b_s}$ as a consequence of the new value of the channel width at the free surface.

It is useful to rewrite (2.1) in divergence form:

$$\frac{\partial \mathbf{U}}{\partial t} + \frac{\partial \mathbf{F}}{\partial x} = \mathbf{R} \tag{2.4}$$

with

$$\begin{aligned} \mathbf{U} &= (A, Q)^T \\ \mathbf{F} &= (Q, \frac{Q^2}{A} + gI_1)^T \\ \mathbf{R} &= (0, gI_2 + gA(S_0 - S_f))^T, \end{aligned}$$

since this displays the conservative character of the system in the absence of source terms. The Jacobian matrix of the system is

$$\mathbf{A} = \frac{\partial \mathbf{F}}{\partial \mathbf{U}} = \begin{pmatrix} 0 & 1 \\ c^2 - u^2 & 2u \end{pmatrix},$$

where $u = Q/A$. The eigenvalues and eigenvectors of A are:

$$\begin{aligned} a^{1,2} &= u \pm c \\ \mathbf{e}^{1,2} &= (1, u \pm c)^T. \end{aligned}$$

3 The method of solution

3.1 Implicit numerical scheme

In (Yee 1986, 1987) a one-parameter family of symmetric explicit and implicit TVD schemes was developed following previous results, and declared as able to be used for time-accurate or steady state calculations. The mathematical theory supporting those TVD schemes refers to scalar equations. The extension to non-linear systems must be done in an ad hoc way following the guide provided by the scalar theory. Starting from the scalar equation

$$\frac{\partial u}{\partial t} + \frac{\partial f}{\partial x} = 0$$

a spatial discretization on a N point regular mesh, $x_{i+1} = x_i + \Delta x, i = 1, N-1$, leads to a system of ODE's:

$$\frac{\partial u_i(t)}{\partial t} = RHS_i(t)$$

where $RHS_i(t)$ represents the residual from the discretization of the spatial derivative at node i of the spatial discretization. The application of the following time integration scheme

$$\frac{u_i^{n+1} - u_i^n}{\Delta t} = \theta RHS_i^{n+1} + (1-\theta)RHS_i^n \qquad 0 \le \theta \le 1$$

provides an implicit formula where n and $n+1$ are the two time levels involved. Except for the value $\theta = 1/2$ it is a first order in time discretization. Another way of expressing it is

$$\frac{u_i^{n+1} - u_i^n}{\Delta t} + \frac{1}{\Delta x}[\theta(f^*_{i+1/2} - f^*_{i-1/2})^{n+1} + (1-\theta)(f^*_{i+1/2} - f^*_{i-1/2})^n] = 0 \qquad (3.1)$$

where the numerical flux $f^*_{i+1/2}$ is responsible for the spatial discretization and has to be specified.

The numerical flux that has been chosen is the one coming from the TVD version of a centred scheme without the term responsible for the space-time combined discretization. It has been recommended in the literature (Yee, 1987) and can be written as

$$f^{*n}_{i+1/2} = \frac{1}{2}[f^n_{i+1} + f^n_i - (1 - \phi(r^n_{i+1/2}))\left|\tilde{a}^n_{i+1/2}\right| \delta u^n_{i+1/2}].$$

In the above expression, $\delta u^n_{i+1/2} = u^n_{i+1} - u^n_i$, $\tilde{a}^n_{i+1/2}$ is the approximate advection speed between points i and i+1, and $\phi(r)$ stands for one of the limiting functions well described in the literature (Sweby, 1984).

The extension of this scheme to the system of equations (2.4) will be presented next. It takes basically two different steps. First, the corresponding vectorial numerical flux must be properly defined by means of an approximate Jacobian matrix. Then the numerical flux has to be adequately approximated at time level n+1 so as to obtain a linear system of discrete equations.
The general formula for the implicit scheme applied to system (2.4) is

$$\frac{\mathbf{U}^{n+1}_i - \mathbf{U}^n_i}{\Delta t} + \frac{1}{\Delta x}[\theta\delta^-(\mathbf{F}^{*n+1}_{i+1/2}) + (1-\theta)\delta^-(\mathbf{F}^{*n}_{i+1/2})] = \theta\mathbf{R}^{n+1}_i + (1-\theta)\mathbf{R}^n_i \quad (3.2)$$

with $\delta^-(\mathbf{F}^{*n}_{i+1/2}) = \mathbf{F}^{*n}_{i+1/2} - \mathbf{F}^{*n}_{i-1/2}$.

The numerical flux $\mathbf{F}^*_{i+1/2}$ is constructed making use of the approximated Jacobian matrix $\tilde{\mathbf{A}}_{i+1/2}$ as

$$\mathbf{F}^*_{i+1/2} = \frac{1}{2}[\mathbf{F}_{i+1} + \mathbf{F}_i - \sum_{k=1,2} \psi^k_{i+1/2}(1 - \phi(r^k_{i+1/2}))\alpha^k_{i+1/2}\tilde{\mathbf{e}}^k_{i+1/2}].$$

The function $\psi^k_{i+1/2}$ is the correction of the eigenvalues $\tilde{a}^k_{i+1/2}$ of $\tilde{\mathbf{A}}_{i+1/2}$ that guarantees the physically valid discontinuities in the solution. In the same way, $\tilde{\mathbf{e}}^k_{i+1/2}$ represents the eigenvectors of the approximate Jacobian and $\alpha^k_{i+1/2}$ are the coefficients of the decomposition of $\delta\mathbf{U}_{i+1/2}$ in that basis. The argument of the limiting function ϕ is

$$r^k_{i+1/2} = \frac{\tilde{a}^k_{i+1/2-s}\alpha^k_{i+1/2-s}}{\tilde{a}^k_{i+1/2}\alpha^k_{i+1/2}} \qquad s = sign(\tilde{a}^k_{i+1/2})$$

The approximate Jacobian can be expressed in its diagonal form as

$$\tilde{\mathbf{A}}_{i+1/2} = \tilde{\mathbf{P}}_{i+1/2}\mathbf{diag}(\tilde{a}^k_{i+1/2})\tilde{\mathbf{P}}^{-1}_{i+1/2}$$

with $\tilde{\mathbf{P}}_{i+1/2}$ the matrix of column eigenvectors. Then it is convenient to define the matrix $\mathbf{B}_{i+1/2}$ as

$$\mathbf{B}_{i+1/2} = \tilde{\mathbf{P}}_{i+1/2}\Lambda_{i+1/2}\tilde{\mathbf{P}}^{-1}_{i+1/2},$$

with $\Lambda_{i+1/2} = \mathbf{diag}[\psi^k_{i+1/2}(1-\phi^k_{i+1/2})]$. The components of B are

$$\mathbf{B} = \frac{1}{\tilde{a}^2 - \tilde{a}^1}\begin{pmatrix} d^1\tilde{a}^2 - d^2\tilde{a}^1 & d^2 - d^1 \\ \tilde{a}^2\tilde{a}^1(d^1 - d^2) & d^2\tilde{a}^2 - d^1\tilde{a}^1 \end{pmatrix},$$

where d^1, d^2 are the two non-zero elements of Λ.

This allows a more compact version of the numerical flux

$$\mathbf{F}^*_{i+1/2} = \frac{1}{2}[\mathbf{F}_{i+1} + \mathbf{F}_i - \mathbf{B}_{i+1/2}\delta\mathbf{U}_{i+1/2}]$$

We are going to start the second stage by proceeding to approximate the source terms at time level n+1. Taking into account that $\mathbf{R}^{n+1}$ contains non-linear dependence in $\mathbf{U}$, the following Taylor's expansion is made

$$\mathbf{R}^{n+1}_i = \mathbf{R}^n_i + \mathbf{G}^n_i\Delta\mathbf{U}_i + O(\Delta t^2)$$

where $\Delta\mathbf{U}_i$ is the time increment to $\mathbf{U}_i$ and $\mathbf{G}$ is the Jacobian matrix of $\mathbf{R}$ which, for the case of a rectangular and prismatic channel with the friction term defined in (2.3), is

$$\mathbf{G} = \begin{pmatrix} 0 & 0 \\ g[S_0 + S_f(1 + \frac{4}{3}\frac{b}{b+2h})] & -\frac{2gA}{Q}S_f \end{pmatrix}.$$

In order to retain a conservative discretization in the implicit part the numerical flux is linearised in the same way

$$\mathbf{F}_i^{n+1} = \mathbf{F}_i^n + \mathbf{A}_i^n \Delta \mathbf{U}_i + O(\Delta t^2)$$

and the following approximation is also made:

$$\mathbf{B}_{i+1/2}^{n+1} = \mathbf{B}_{i+1/2}^n$$

The introduction of these two simplifications in (3.2) allows us to write it in the form of a block tridiagonal system

$$\mathbf{AA}_i \Delta \mathbf{U}_{i-1} + \mathbf{BB}_i \Delta \mathbf{U}_i + \mathbf{CC}_i \Delta \mathbf{U}_{i+1} = \mathbf{DD}_i \quad i = 2, 3, ..., N-1 \tag{3.3}$$

in which the coefficients are 2x2 matrices with the following elements:

$$\begin{aligned}
\mathbf{AA}_i &= -\frac{\lambda\theta}{2}[\mathbf{A}_{i-1} + \mathbf{B}_{i-1/2}]^n \\
\mathbf{BB}_i &= \mathbf{I} - \theta\Delta t \mathbf{G}_i^n + \frac{\lambda\theta}{2}[\mathbf{B}_{i+1/2} + \mathbf{B}_{i-1/2}]^n \\
\mathbf{CC}_i &= \frac{\lambda\theta}{2}[\mathbf{A}_{i+1} - \mathbf{B}_{i+1/2}]^n \\
\mathbf{DD}_i &= -\lambda(\mathbf{F}_{i+1/2}^* - \mathbf{F}_{i-1/2}^*)^n + \Delta t \mathbf{G}_i^n
\end{aligned}$$

where $\lambda = \Delta t / \Delta x$.

The presented scheme is a second order in space and first order in time conservative discretization. It offers greatest advantages for the calculation of steady solutions. It is advisable to choose $\theta = 1$ and make zero the limiting functions contained in the implicit part. This renders the implicit operator only first order in space but allows bigger CFL values.

3.2 Boundary Conditions

The tridiagonal system (3.3) that has been obtained from the implicit scheme is written only for the grid points $i = 2, 3..., N-1$. It must be completed by means of the boundary conditions. They will be linearised to provide two matrix

equations of the form,

$$\mathbf{BB}_2\Delta\mathbf{U}_1 + \mathbf{CC}_2\Delta\mathbf{U}_2 = \mathbf{DD}_2 \tag{3.4}$$

and

$$\mathbf{AA}_{N-1}\Delta\mathbf{U}_{N-1} + \mathbf{BB}_{N-1}\Delta\mathbf{U}_N = \mathbf{DD}_{N-1}, \tag{3.5}$$

using some information coming from the theory of characteristics and some from the imposed boundary conditions.

A number of alternative strategies, some of them specially recommended for steady state calculations (see Yee 1981 and Alcrudo 1992), were tried for implementing the boundary conditions, but the following procedure was found to be the most reliable.

In order to illustrate the technique, let us take the example of a subcritical upstream case with discharge imposed as the external boundary condition

$$Q_1 = f(t).$$

It is clear then that

$$\Delta Q_1 = Q_1 - Q_1^n$$

is a known value and that it is independent of the rest of the points.

To work out an expression for ΔA we start from the following form of the characteristic equations

$$\frac{DQ}{Dt} + (-\frac{Q}{A} \pm \sqrt{gA/b})\frac{DA}{Dt} = 0 \tag{3.6}$$

which are known to hold along lines

$$\frac{dx}{dt} = \frac{Q}{A} \pm \sqrt{gA/b}.$$

The integration of (3.6) can be achieved numerically by means of an iterative procedure (see Garcia-Navarro and Savirón 1991). The first iteration can be used to implement a non-expensive approach for the boundary problem of our implicit problem.

From the upstream component of (3.6) the following can be written

$$Q_1^{n+1} - Q_r^n + (-\frac{Q_r^n}{A_r^n} - \sqrt{gA_r^n/b})(A_1^{n+1} - A_r^n) = 0.$$

In the above expression, r stands for the point at the foot of the characteristic in the old time level. It can be rewritten as

$$Q_1^{n+1} = CA_1^{n+1} + D \tag{3.7}$$

with

$$C = (\frac{Q_r^n}{A_r^n} + \sqrt{gA_r^n/b})$$
$$D = Q_r^n - CA_r^n$$

This linear relation is to be used as the one complementing the external boundary condition. The expression of ΔA at the boundary is then

$$\Delta A_1 = A_1^{n+1} - A_1^n$$

where

$$A_1^{n+1} = \frac{Q_1^{n+1} - D}{C}.$$

This enables us to write an expression like (3.4) with

$$\mathbf{BB}_2 = \begin{pmatrix} 1 & 0 \\ 0 & 1 \end{pmatrix} \quad \mathbf{CC}_2 = \begin{pmatrix} 0 & 0 \\ 0 & 0 \end{pmatrix} \quad \mathbf{DD}_2 = \begin{pmatrix} \Delta A_1 \\ \Delta Q_1 \end{pmatrix}.$$

It becomes a simplified version if point 2 is used as the intermediate point r. This approach avoids interpolation and even though it implies a loss of accuracy, it has proved to give satisfactory results even for the problems with transients at the boundaries.

3.2.1 Internal boundary conditions

The problem of the numerical treatment of internal boundary conditions will appear in this work when solving problems of flow in a pipe or channel junction. The basic idea is essentially the same as the one applied to the external boundaries. The $kmax$ points involved in the junction problem are end points of the pipes/channels meeting at that junction, so that a linear relation between Q and A like (3.7)(or an analogous one between Q and h), can be written for each of them.

The conditions imposed at the junction are of two kinds, normal junction:

$$\sum_{k=1}^{kmax} Q_k = 0$$

$$h_1 = h_2 = ... = h_{kmax} = H$$

or a well junction, in which a storage well of top area A_w and depth H_w is assumed,

$$\sum_{k=1}^{k} maxQ_k = A_w \frac{dH_w}{dt}$$

$$h_1 = h_2 = ... = h_{kmax} = H_w = H.$$

The solution in both cases reduces to calculate

$$H = \frac{A_w H_w^n + \Delta t \sum D_k}{A_w - \Delta t \sum C_k}$$

and then make use of the linear relations to determine the $kmax$ different discharges

$$Q_k = C' h_k + D' \quad k = 1, kmax$$

with, in this case,

$$C' = b(\frac{Q_r^n}{A_r^n} + \sqrt{gA_r^n/b})$$

$$D' = Q_r^n - C' h_r^n$$

the subscript r referring again to the immediate point in the interior of each pipe.

3.3 System solver

Once the boundary conditions have been used to produce a complete block tridiagonal system of equations in terms of the time increments of the variables, which will be denoted as $\mathbf{X}_i$ in this section, a block version of the Thomas algorithm is used to obtain the solution as follows.

The system of equations has the property that if

$$\mathbf{X}_{i-1} = \gamma_{i-1} - \alpha_{i-1}\mathbf{X}_i$$

holds for a couple of points $i-1, i$, then it is also true for the next pair $i, i+1$ and hence for all the rest of points, and it is possible to use the following recurrence:

$$\alpha_i = (\mathbf{BB}_i - \mathbf{AA}_i\alpha_{i-1})^{-1}\mathbf{CC}_i$$

$$\gamma_i = (\mathbf{BB}_i - \mathbf{AA}_i\alpha_{i-1})^{-1}(\mathbf{DD}_i - \mathbf{AA}_i\gamma_{i-1})$$

It is then convenient to cast the upstream block equation (3.4) in the form

$$\mathbf{X}_1 = \gamma_1 - \alpha_1\mathbf{X}_2.$$

This will provide the starting values (γ_1, α_1). Using the above recurrence all the couples (γ_i, α_i) can be next obtained. The last of the equations we can write is

$$\mathbf{X}_{N-1} = \gamma_{N-1} - \alpha_{N-1}\mathbf{X}_N, \tag{3.8}$$

which relates the two last points in a linear way with known coefficients. If the independent relation between them (3.5) is also considered, the system of two

equations can be used to eliminate $\mathbf{X}_{N-1}$ and calculate $\mathbf{X}_N$. Once $\mathbf{X}_N$ is known, the relation (3.6) is the departure point of a backwards sweep leading to all the $\mathbf{X}_i$'s up to $\mathbf{X}_1$.

4 Idealised test problems

4.1 Steady State in a channel

The advantages of using the presented approach for the calculation of steady open channel flow profiles were already pointed out in Garcia-Navarro and Alcrudo 1992, where quantitative results for the convergence rates were provided. Here, some examples of steady solutions obtained through unsteady calculations in open channels are first presented.

Figs. 1 and 2 show two solutions of flow over a bump. Starting from uniform initial conditions in water level and discharge, a constant head imposed at the upstream boundary and a fixed water level at the downstream end lead to the equilibrium state. In Fig.1, water accelerates to reach critical conditions over the bump and becomes supercritical downstream, were nothing is imposed. In Fig.2, the same situation is connected by a hydraulic jump to the imposed downstream water level. Both examples have been computed on a 80 point grid using a CFL=100. The numerical solution has been plotted together with a continuous line representing the exact solution.

Figs. 3 and 4 correspond to two steady profiles in a sloping channel. The discharge in both is $Q = 3m^3/s$ and the slope $S_0 = 0.001$. The initial conditions were the same discharge $Q_0 = 3m^3/s$ and a uniform water depth $h_0 = 2m$. Constant discharge upstream and a fixed water level downstream give rise to a subcritical profile in the first example, with $n = 0.03$ (Fig.3) and to a discontinuous solution in the second example, in which $n = 0.009$ (Fig.4). The calculation was done on a grid with N = 100 using a CFL=50. The continuous line appearing in Fig.4 is a comparison with the numerical solution provided by Roe's second order explicit scheme (see Baines et al. 1992).

4.2 Dam break problem

Even though the class of implicit schemes presented was devised to cope with strong discontinuities in gas-dynamics steady state problems, the conservative linearization applied has been said to render it suitable also for unsteady calculations. In river and pipe flows, discontinuities are generally weaker, so the idealised dambreak problem was chosen because it is a classical example of non-linear flow with shocks to test accuracy and conservation in numerical schemes since it has an analytical solution.

This problem is generated by the homogeneous one-dimensional shallow water equations with the initial conditions

$$\begin{aligned} h(x,0) &= \begin{cases} h_L & \text{if } x \leq \frac{L}{2} \\ h_R & \text{if } x > \frac{L}{2} \end{cases} \\ Q(x,0) &= 0. \end{aligned}$$

If the calculation times used are so as to avoid interaction with the extremities of the channel, the boundary conditions are trivial.

Figs. 5-8 are a sample of the solution obtained through the solution of this test problem for two different values of the initial height ratio $h_L : h_R$. Figs. 5 and 6 represent the profiles of the water surface after the dambreak in the 5:1 case for four different CFL values as computed on two grids of 50 and 100 cells respectively. Figs. 7 and 8 are the equivalent for the 20:1 case. The analytic solution appears as a continuous line.

For the higher CFL values, a linear increase in the value of Δt was used in order to overcome the difficulty imposed by the initial discontinuity when using a very large initial time step.

5 More realistic test problems

5.1 Pressurisation in a single pipe

As suggested in Baines et al. 1992, the numerical results obtained using the presented implicit scheme are now compared with experimental data for a horizontal, rough, closed channel. As described in Wiggert 1978, it is a 10m long pipe. The width of the pipe is b =0.51m, the height is 0.148m and the slot's width above that is b_s =0.01m. The roughness coefficient is $n = 0.012$. The initial conditions are $Q_0 = 0$ and $h_0 = 0.128$m.

Then a wave coming from the left side causes the closed channel to pressurise. The upstream boundary condition is a given hydrograph and the downstream boundary condition is a fixed water level, $h_L = 0.128$m. Starting from upstream, the pressurization moves downstream as a front wave.

Figs. 9 and 10 show results of the variation in time of water level at x = 3.5m. The horizontal line in all of them represents the channel soffit, the continuous line corresponds to the numerical results provided by the implicit scheme, whilst the circles are the values from Wiggert 1978. Fig. 9 displays results on a grid of 20 points, that is, with Δx =0.5m., and Fig. 10 with Δx =0.125m, for different values of the time step.

5.2 Transient flow in a junction

Some cases of numerical simulation of the evolution of flow towards the steady state with different dynamic states of the flow at the junction are now presented.

We have considered a prismatic channel 1m wide (channel 1) branching into two channels of the same geometry (channels 2 and 3). Each of the channels is discretized using a constant Δx. The initial discharges are assigned so as to ensure mass conservation at the junction and the initial water depth is supposed uniform. The discharge will be prescribed at the inlet point to channel

1 and a weir type or zero first derivative boundary condition will be applied at the outlet of channels 2 and 3. The internal boundary conditions imposed at the junction will be the simplest ones to ensure continuity.

$$\text{Subcritical flow} \quad : \quad \begin{cases} (Q1)_N = (Q2)_1 + (Q3)_1 \\ (h1)_N = (h2)_1 \\ (h1)_N = (h3)_1 \end{cases}$$

$$\text{Supercritical flow} \quad : \quad \begin{cases} (Q2)_1 = (Q3)_1 = \frac{1}{2}(Q1)_N \\ (h1)_N = (h2)_1 \\ (h1)_N = (h3)_1 \end{cases}$$

The steady state shown in Fig. 11 was reached starting from the initial conditions

$$\begin{cases} (Q1)_i = 3m^3/s \\ (Q2)_i = (Q3)_i = 1.5m^3/s \\ (hj)_i = 2m \quad j = 1, 2, 3 \end{cases}$$

in a system of channels of bottom slopes $S_{01} = 0.01$, $S_{02} = S_{03} = 0.001$ and uniform Manning coefficient n= 0.009. The equilibrium flow is subcritical at the junction but discontinuous in pipe 1, where a hydraulic jump connects the two regimes. The boundary conditions, common to both examples, are a constant upstream discharge and a 2m high downstream weir.

In the second example, Fig.12, the values of the bed slopes are $S_{01} = S_{02} = S_{03} = 0.01$. The initial conditions as well as the roughness were the same as in the previous example. The flow is now supercritical all over the system except for the downstream part of pipes 2 and 3, in which identical hydraulic jumps have developed to connect with the downstream boundary condition.
The space step used was Δx= 4m, and, as time step, the one given by a CFL = 10.

As proposed in Wixcey 1990, a system of 5000m long pipes with slopes $S_{01} = 0.002$ and $S_{02} = S_{03} = 0.001$ and friction coefficient $n = 0.01$ shall

be considered now. Initially, a steady state is obtained starting from the initial conditions

$$\begin{cases} (Q1)_i = 0.1 m^3/s \\ (Q2)_i = (Q3)_i = 0.05 m^3/s \\ (h1)_i = (h2)_i = (h3)_i = 0.2m \end{cases}$$

and holding constant the inflow discharge at $(Q1)_1 = 0.1 m^3/s$ on a grid with Δx= 50m. A saw tooth of peak value Q_M and period τ= 600s is enforced in the upstream end of pipe 1. In Figs. 13-17, time histories of discharge and depth at locations corresponding to i = N/10, N/5 and N after ten periods have been recorded.

Figs. 13 and 14 are the discharges and depths respectively for the case Q_M= $2.8 m^3/s$ using a value of CFL=1. Fig. 15 shows the equivalent discharge plot for the case of CFL=4.

Figs. 16 and 17 are water depth histories following a peak discharge Q_M= $3.2 m^3/s$ that produces pressurization in the first part of pipe 1. Fig. 16 was obtained with a CFL unity and Fig. 17 with a CFL=2.

5.3 Transient flow in a looped network

One of the main present fields of application of 1-D implicit schemes is the simulation of flow in pipe networks. In this subsection we are going to consider a simple looped network as the one shown in Fig.18 and repeat the numerical tests suggested in Wixcey, 1990.

Each of the pipes is closed, squared, 1m wide and 100m long. They are discretized in 10 intervals. The bottom slopes are $S_{01} = 0.002$, $S_{02} = S_{03} = 0.001$, $S_{04} = 0.0$, $S_{05} = S_{06} = 0.001$ and $S_{07} = 0.002$. Using a uniform value of the friction coefficient n= 0.01, a first calculation is made with the implicit technique to obtain a steady state of the system starting from the initial conditions:

$$\begin{cases} (Q1)_i = 0.1m^3/s \\ (Q2)_i = (Q3)_i = 0.05m^3/s \\ (Q4)_i = 0.0m^3/s \\ (Q5)_i = (Q6)_i = 0.05m^3/s \\ (Q7)_i = 0.1m^3/s \\ (h1)_i = (h2)_i = (h3)_i = (h4)_i = (h5)_i = (h6)_i = (h7)_i = 0.2m, \end{cases}$$

prescribing a constant discharge at the inlet of pipe 1 and using a zero first derivative as downstream boundary condition in pipe 7. Junctions A and D are treated following the procedure described in the previous subsection. A storage well of top surface A_w= 5 m^2 is supposed in junctions B and D. The continuity equation and the condition over the depths at the junction in that case are as described in subsection 3.2.1

The steady state solution has zero discharge in pipe 4 due to the symmetry of the network. It is then used as initial condition to a second calculation.

A sawtooth of peak discharge Q_M and period τ= 600s is enforced in the upstream end for a total of four periods. The time variations of depth and discharge in pipes 1,2,5 and 7 are recorded at grid points $i = N/2$ and $i = N$. Those in pipe 4 are recorded at locations $i = N/10$, $i = N/2$ and $i = 9N/10$. They have been plotted and displayed in Figs. 19-30. The results in pipes 3 and 6 have been omitted because of the system's symmetry.

In Figs. 19-22, the time histories resulting from the application of a maximum Q_M= $2m^3/s$ are presented for different values of the CFL number. The flow remains unpressurized all over the network and, as pointed out by Wixcey, attains a pseudo steady state really noticeable in pipe 4. Note that the discharge at the centre point of that pipe is constantly zero and equal but of different sign in the symmetric points. The results are qualitatively independent of the CFL

number, and consequently the time step size, used. A loss of accuracy is the only consequence.

In Figs. 23-30, the results corresponding to a bigger peak $Q_M = 3m^3/s$ are shown. Pressurisation occurs in this case in pipe 1. The CFL restriction to the value 1 is again not necessary, as the pictures indicate. Some non-physical spikes appear nevertheless for values above 5, indicating that further research is necessary to determine whether there exists a time step restriction in delicate situations.

6 Remarks and comments

A conservative implicit method belonging to a family of TVD schemes has proved to be suitable for the numerical treatment of a great variety of hydraulic problems. It is able to cope with subcritical, supercritical and mixed-regime flows providing accurate results without being restricted by the usual CFL stability condition.

The best results are obtained when applying it to the calculation of continuous or discontinuous steady states, allowing the use of time steps some orders of magnitude bigger than those in the explicit case, and achieving a second order accuracy in space and time.

It is able to handle the unsteady problems that are frequently encountered in channels and pipes, such as front waves and sudden passage from free surface to pressurised flow. It remains stable and accurate provided that the CFL does not become overly large.

The performance of the implicit scheme has been tested in a simplified looped network giving very good results. It is a good candidate for numerical simulation in pipe networks because it keeps the advantages of classical implicit schemes and properly deals with all kinds of flow. No special numerical treatment has been applied in this work, but the block tridiagonal matrix allows for the use

of special techniques such as the condensation method, currently in use in some commercial codes involving implicit methods for pipe networks (Uan 1984 and Fugazza 1990).

7 Acknowledgment

We would like to thank Drs. Mike Baines and Pete Sweby for many useful and interesting discussions during the course of this work.

References

[1] Alcrudo, F., *"Esquemas de Alta Resolucion de Variacion Total Decreciente para el Estudio de Flujos Discontinuos de Superficie Libre."* PhD Thesis, University of Zaragoza, 1992.

[2] Baines, M.J., Maffio A., Di Filippo, A., *"Unsteady 1-D Flows with Steep Waves in Plant Channels: The Use of Roe's Upwind TVD Difference Scheme."* Advances in Water Resources., **15**, pp. 89-94, 1992.

[3] Cunge, J.A., Holly, F.M. and Verwey, A., *"Practical Aspects of Computational River Hydraulics."* Pitman Pub. Inc., 1980.

[4] Fugazza, M., *"Moto Vario in una Rete di Canali Prismatici"* L'Energia Elettrica,**10**, pp. 427-437, 1990.

[5] Garcia-Navarro, P. and Saviron, J.M., *"McCormack's Method for the Numerical Simulation of One-Dimensional Discontinuous Unsteady Open Channel Flow"* Journal of Hydraulic Research,**30**, pp. 95-105, 1992.

[6] Garcia-Navarro, P. and Alcrudo, F., *"Implicit and Explicit TVD Methods for Discontinuous Open Channel Flows"* Proc. of the 2nd Int. Conf. on Hydraulic and Environmental Modelling of Coastal, Estuarine and River Waters, Vol.2, Edited by R.A. Falconer, K. Shiono and R.G.S. Matthew, Ashgate, 1992.

[7] Sweby, P.K., *"High Resolution Schemes using Flux Limiters for Hyperbolic Conservation Laws"* SIAM, Journal of Numerical Analysis **21**, 1984.

[8] Uan, M, *"Principe de Résolution de Modélisations Filaires des Écoulements à Surface Libre. Application à un Réseau Maillé."* EDF Report HE/43-84-40, 1984.

[9] Wiggert, D.C. and Sundquist, M.J., *"Fixed-Grid Characteristics for Pipeline Transients."* Journal of the Hydraulic Division, ASCE,**103**, pp. 1403-1415, 1978.

[10] Wixcey, J.R., *"An Investigation of Algorithms for Open Channel Flow Calculations"* Numerical Analysis Internal Report, **21**, Department of Mathematics, University of Reading, 1990.

[11] Yee, H.C., *"Numerical Approximation of Boundary Conditions with Application to Inviscid Equations of Gas Dynamics."* NASA Technical Memorandum 81265, 1981.

[12] Yee, H.C., *"Linearised Form of Implicit TVD Schemes for the Multidimensional Euler and Navier-Stokes Equation."* Comps. and Maths. with Appls., **12A**, pp. 413-432, 1986.

[13] Yee, H.C., *"Construction of Explicit and Implicit Symmetric TVD Schemes and Their Applications"* Journal of Computational Physics, **68**, pp. 151-179, 1987.

List of Figures

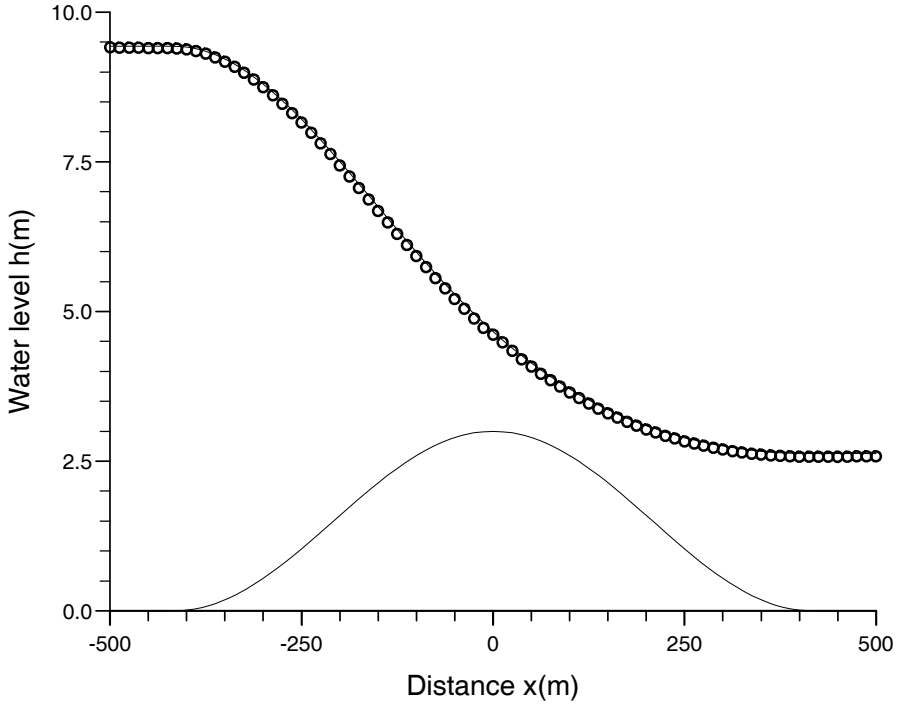

Figure 1: Steady profile over a bump. Supercritical flow.

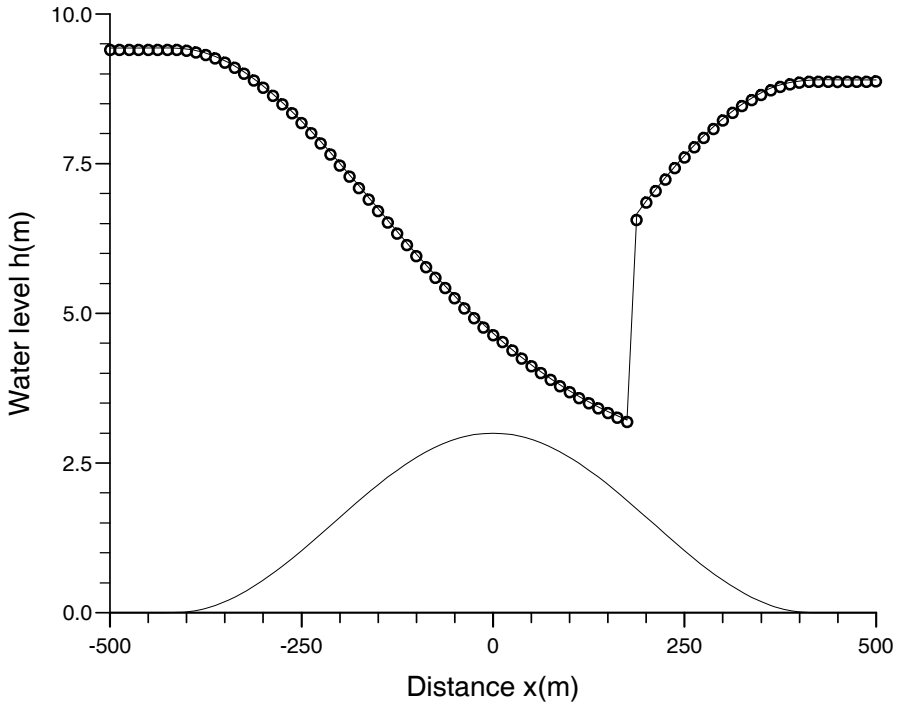

Figure 2: Steady profile over a bump. Mixed flow with hydraulic jump.

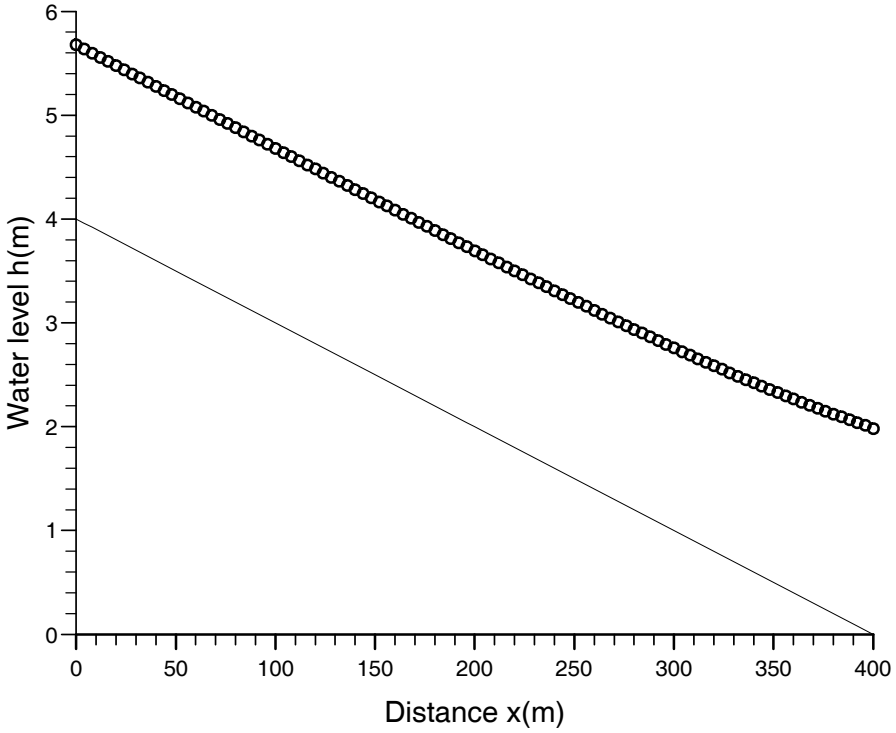

Figure 3: Steady profile in a channel. Subcritical flow.

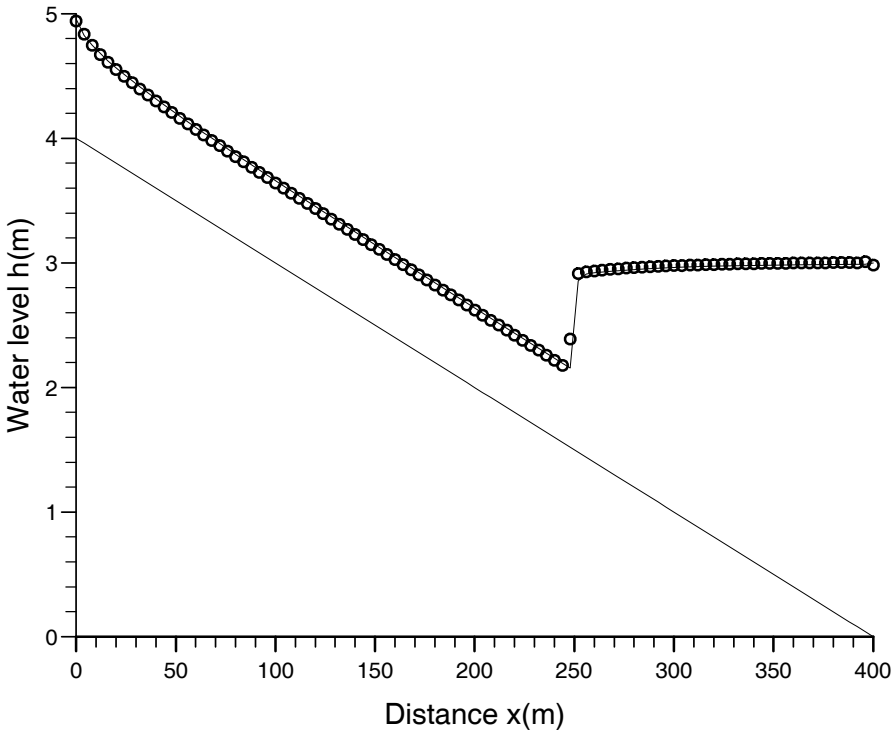

Figure 4: Steady profile in a channel. Mixed flow with hydraulic jump.

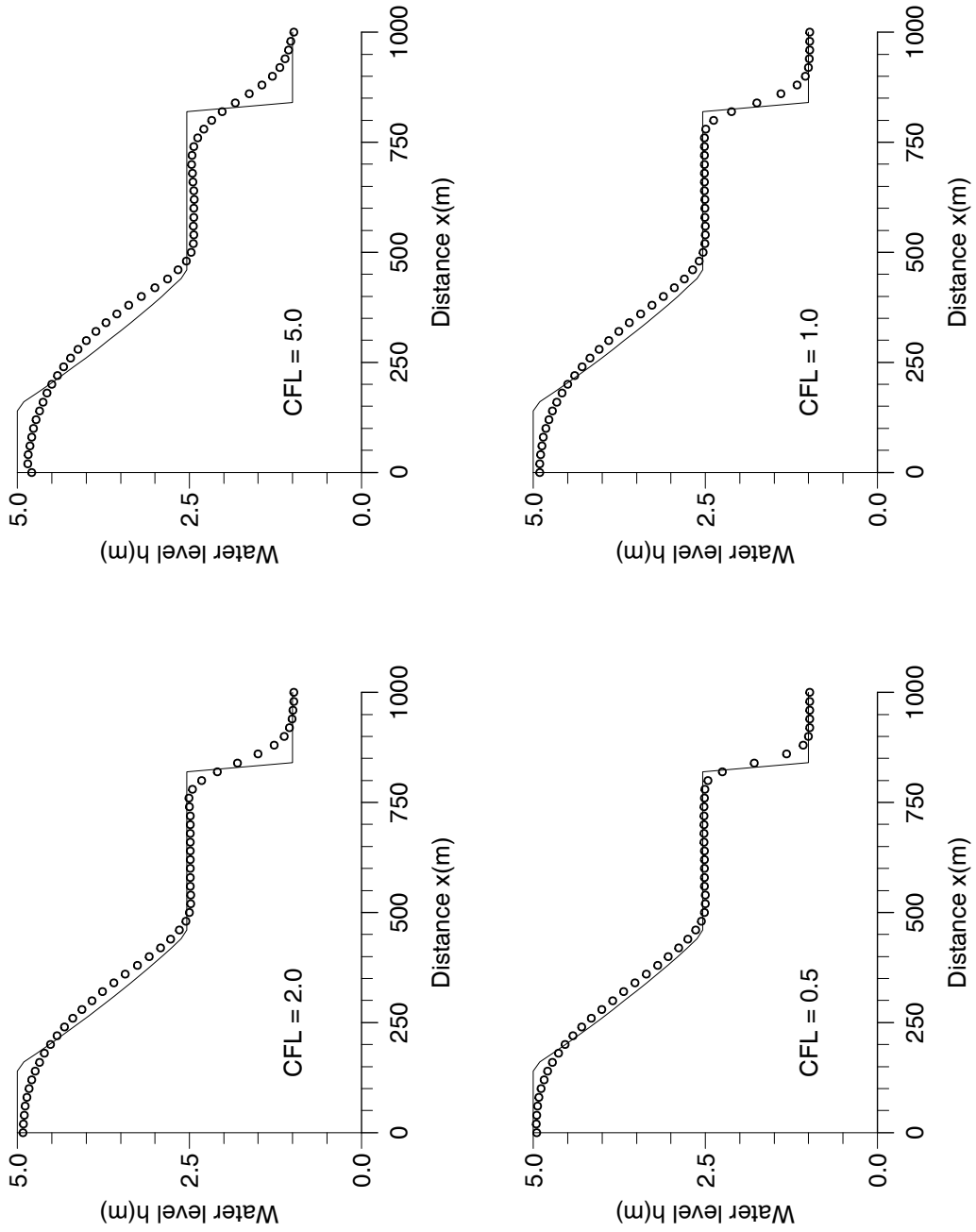

Figure 5: Dam break problem. Initial ratio 5:1. N=51.

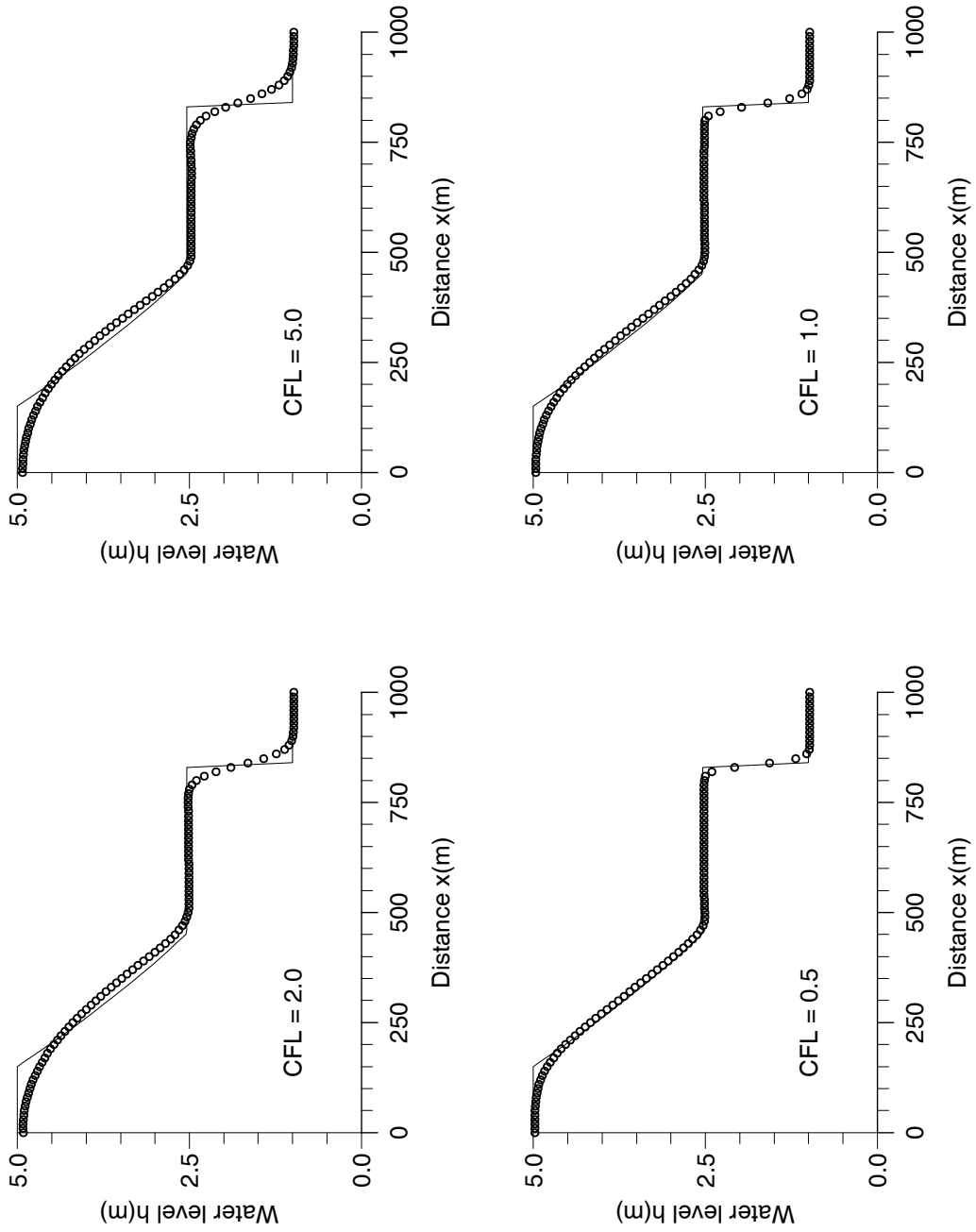

Figure 6: Dam break problem. Initial ratio 5:1. N=101.

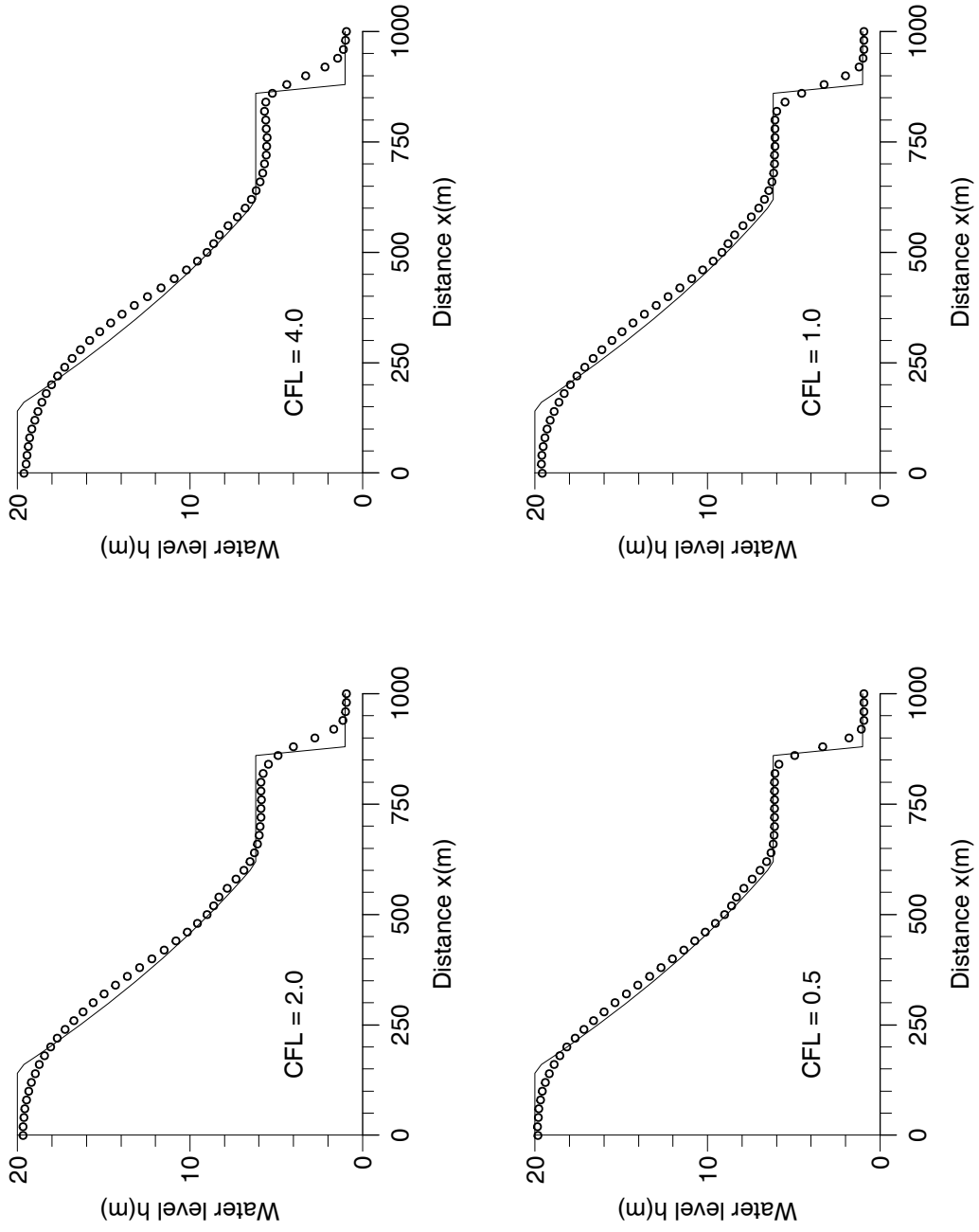

Figure 7: Dam break problem. Initial ratio 20:1. N=51.

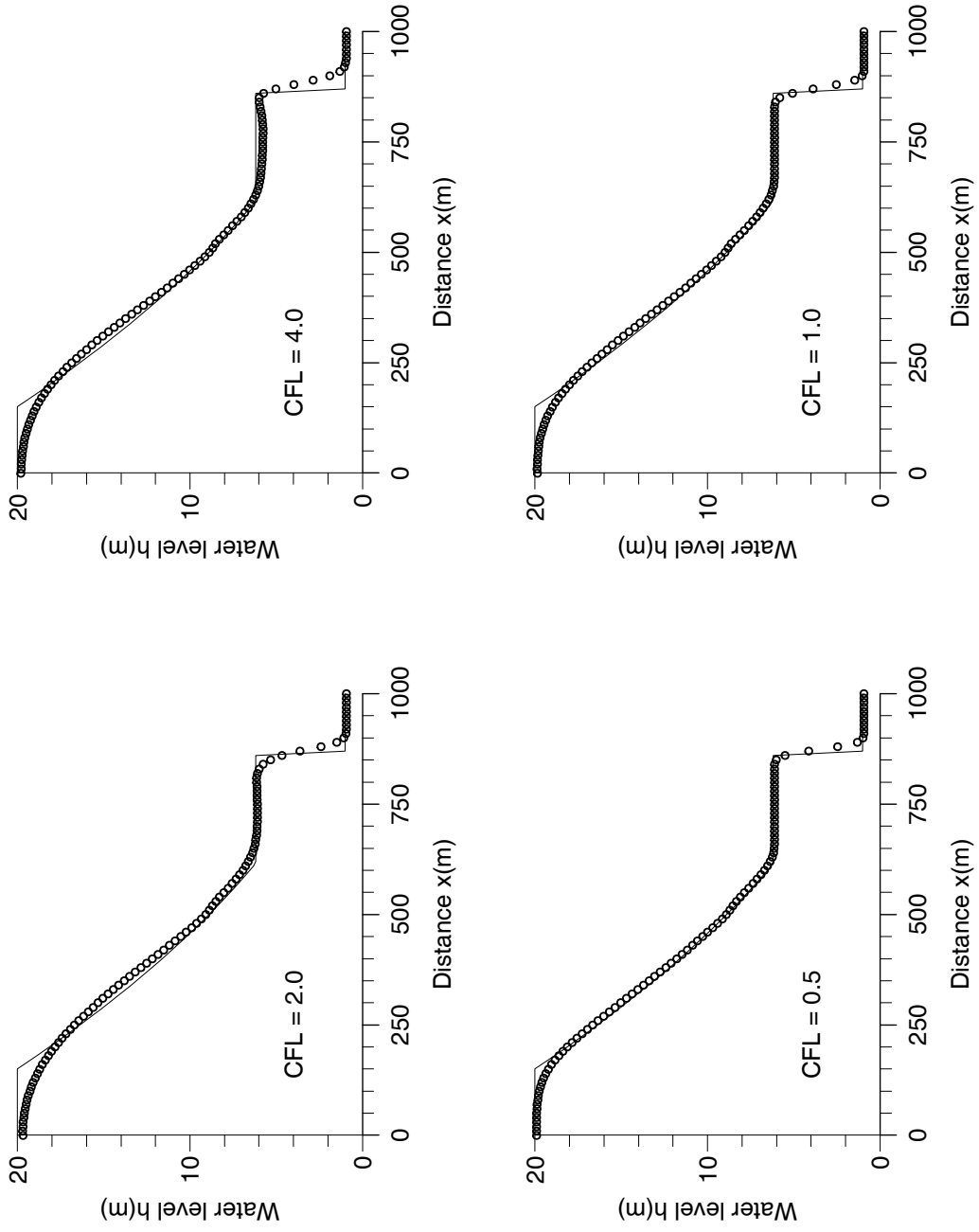

Figure 8: Dam break problem. Initial ratio 20:1. N=101.

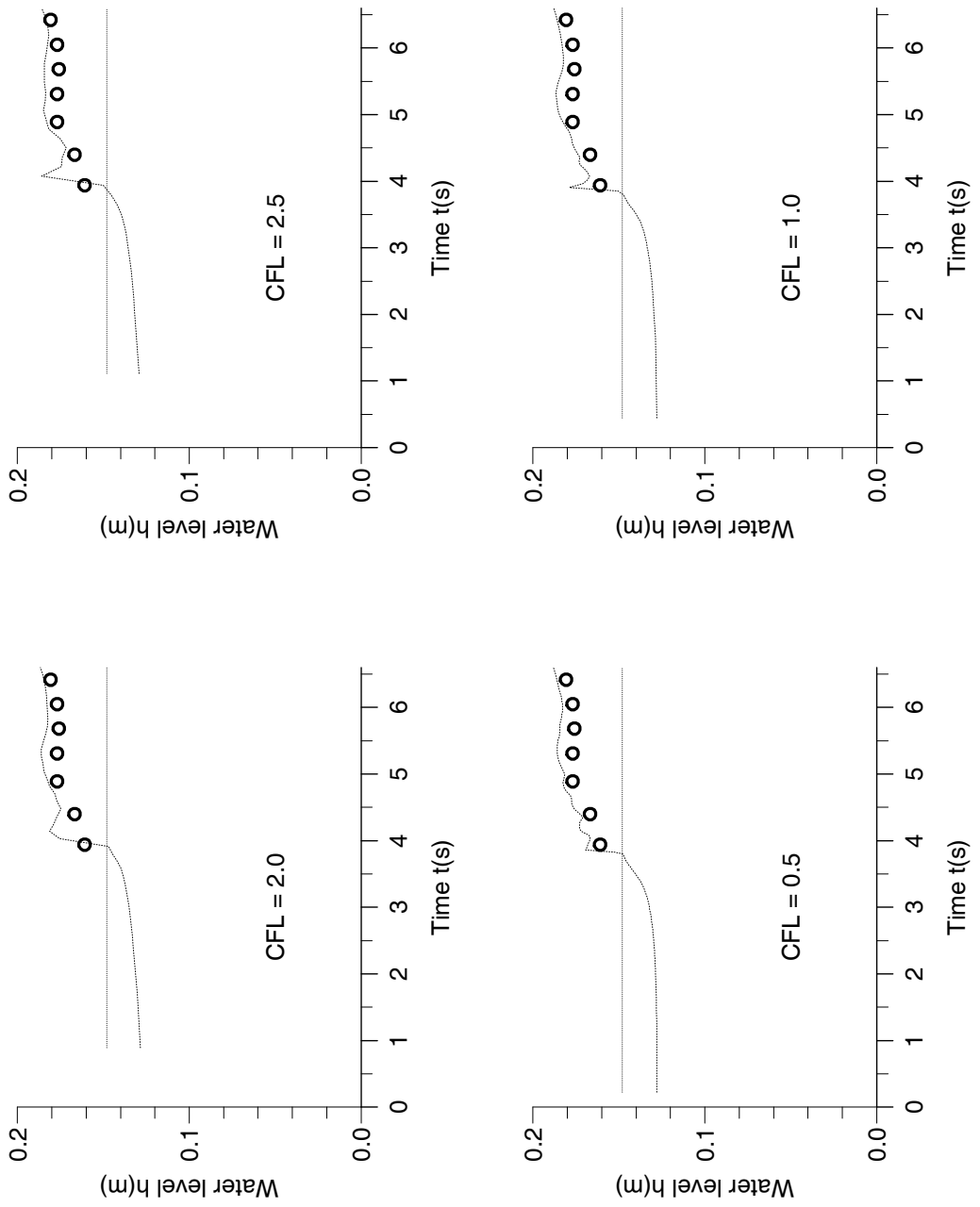

Figure 9: Pressurisation wave in a pipe. Δx=0.5.

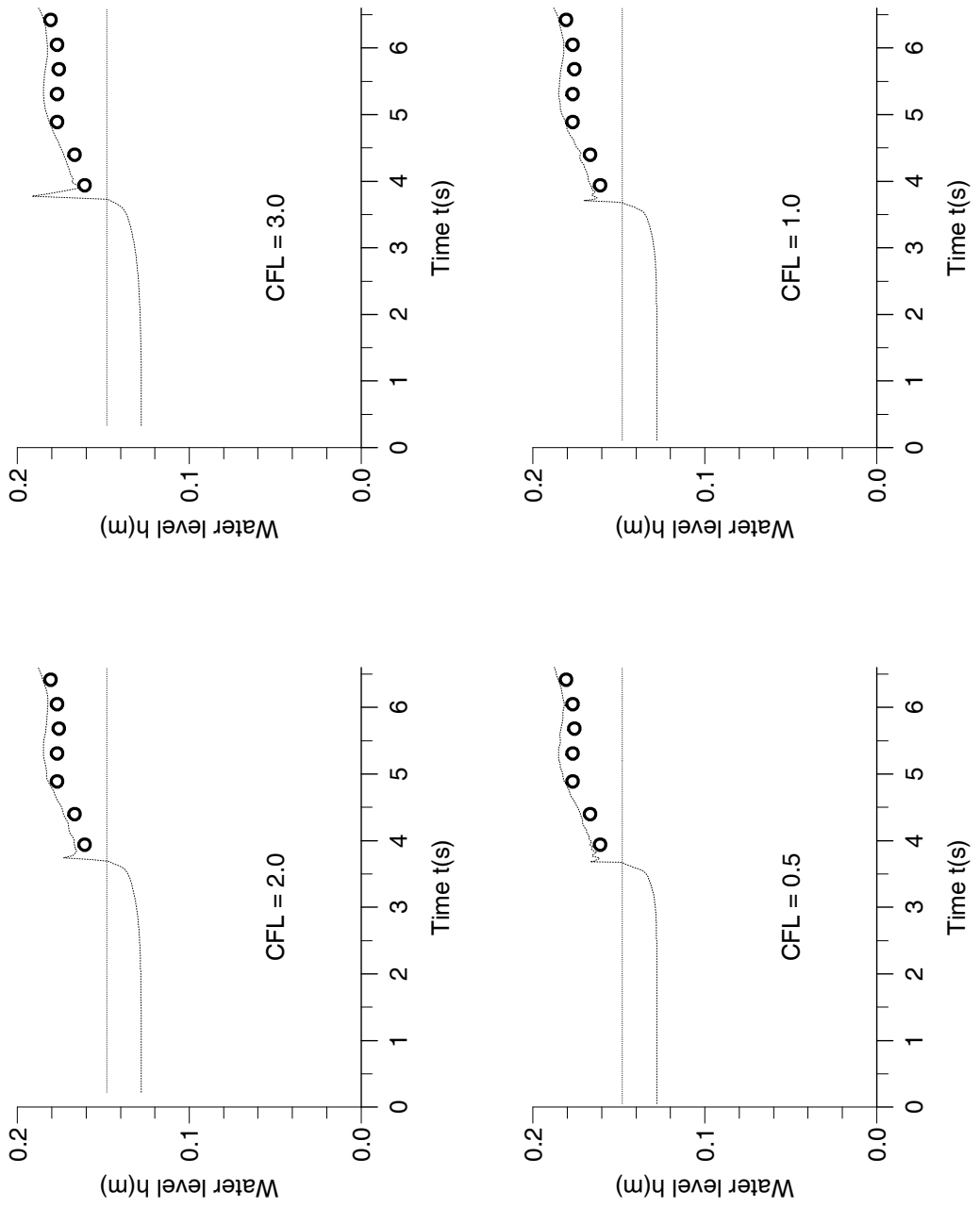

Figure 10: Pressurisation wave in a pipe. Δx=0.125.

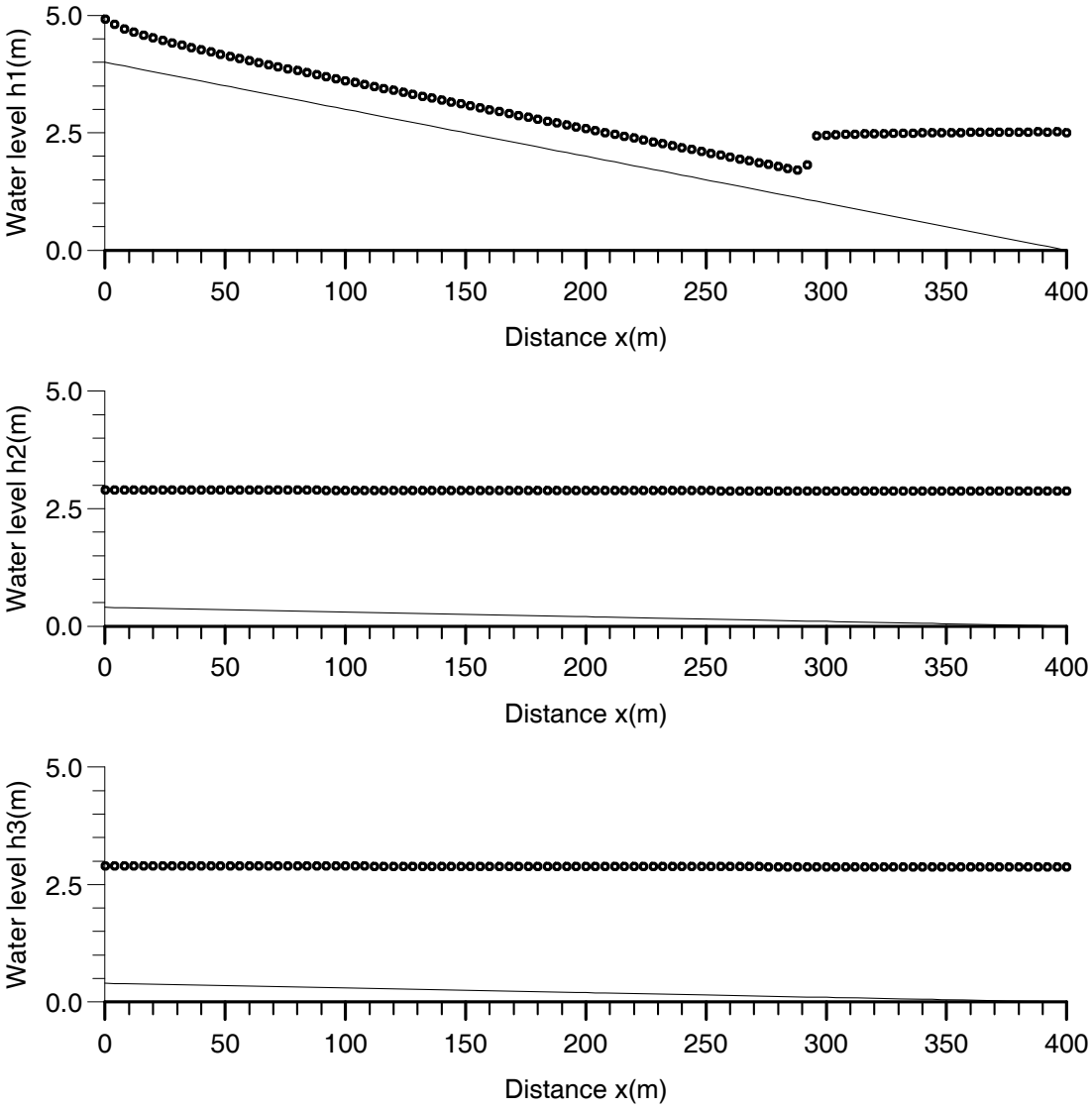

Figure 11: Subcritical flow in a junction with hydraulic jump in the incoming channel.

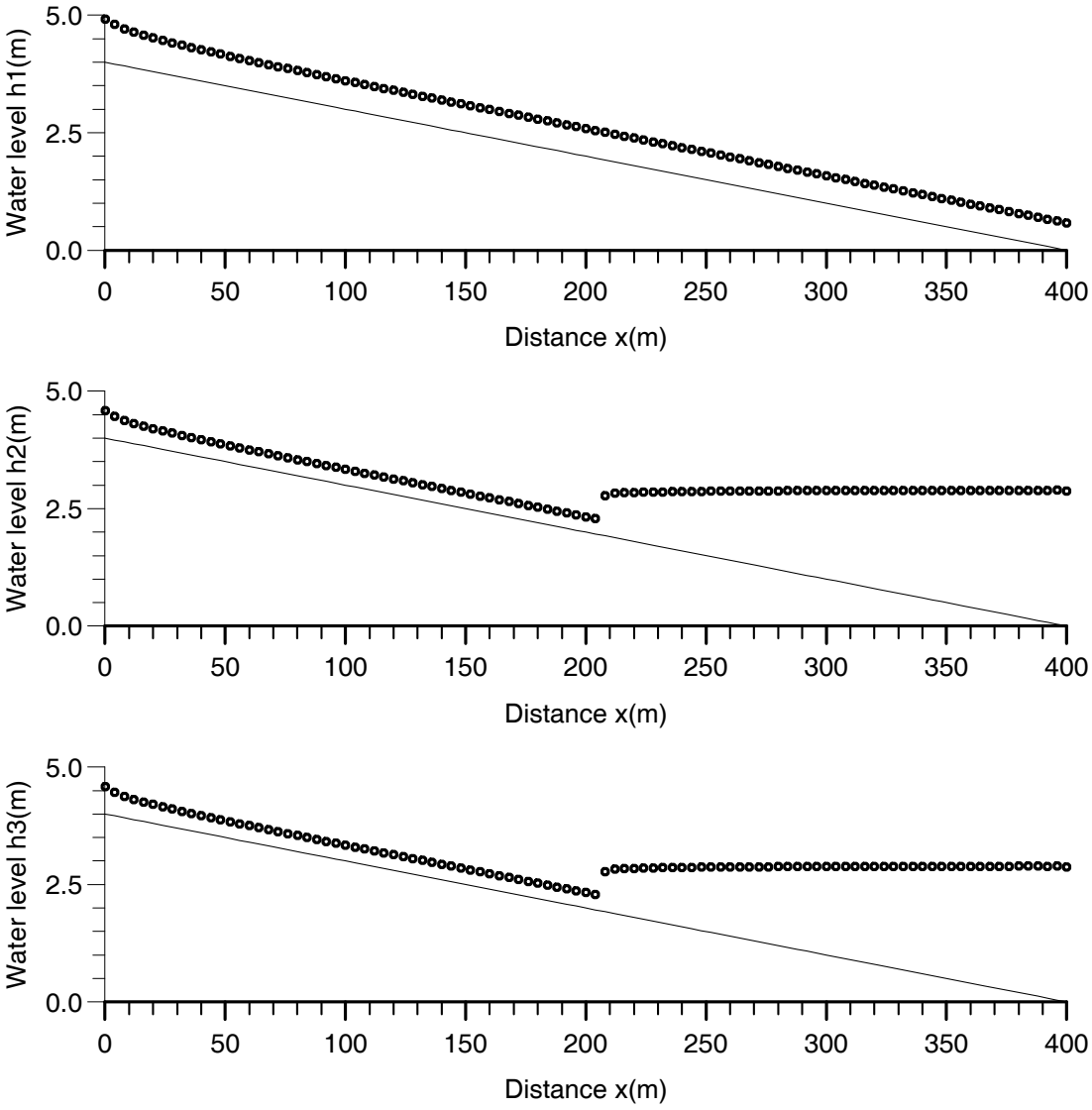

Figure 12: Supercritical flow in a junction with hydraulic jumps in the outgoing channels.

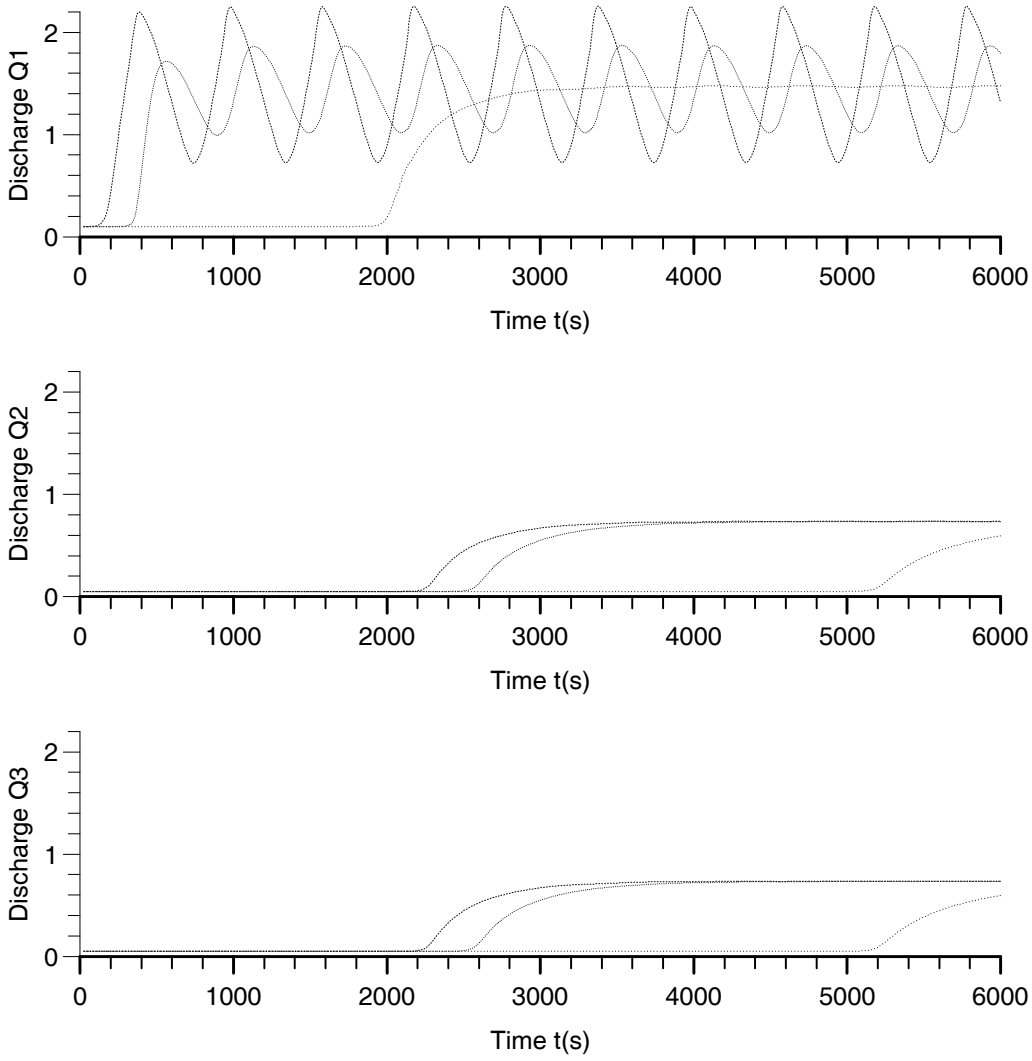

Figure 13: Discharge hydrographs at different locations. Peak value of the inflow wave $Q_M = 2.8m^3/s$. CFL=1. $\Delta x = 50m$. N= 100.

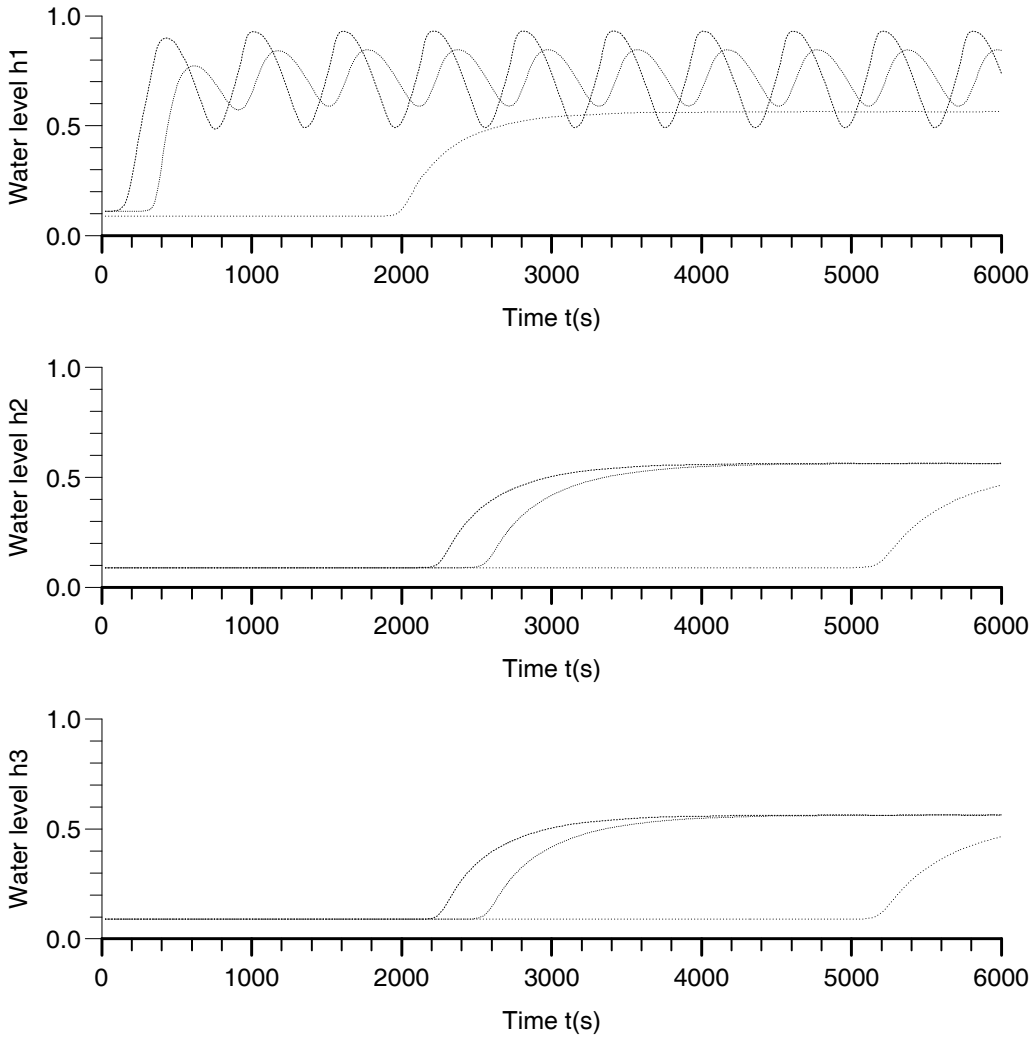

Figure 14: Water level limnigrams at different locations. Peak value of the inflow wave $Q_M = 2.8m^3/s$. CFL=1. $\Delta x = 50m$. N= 100.

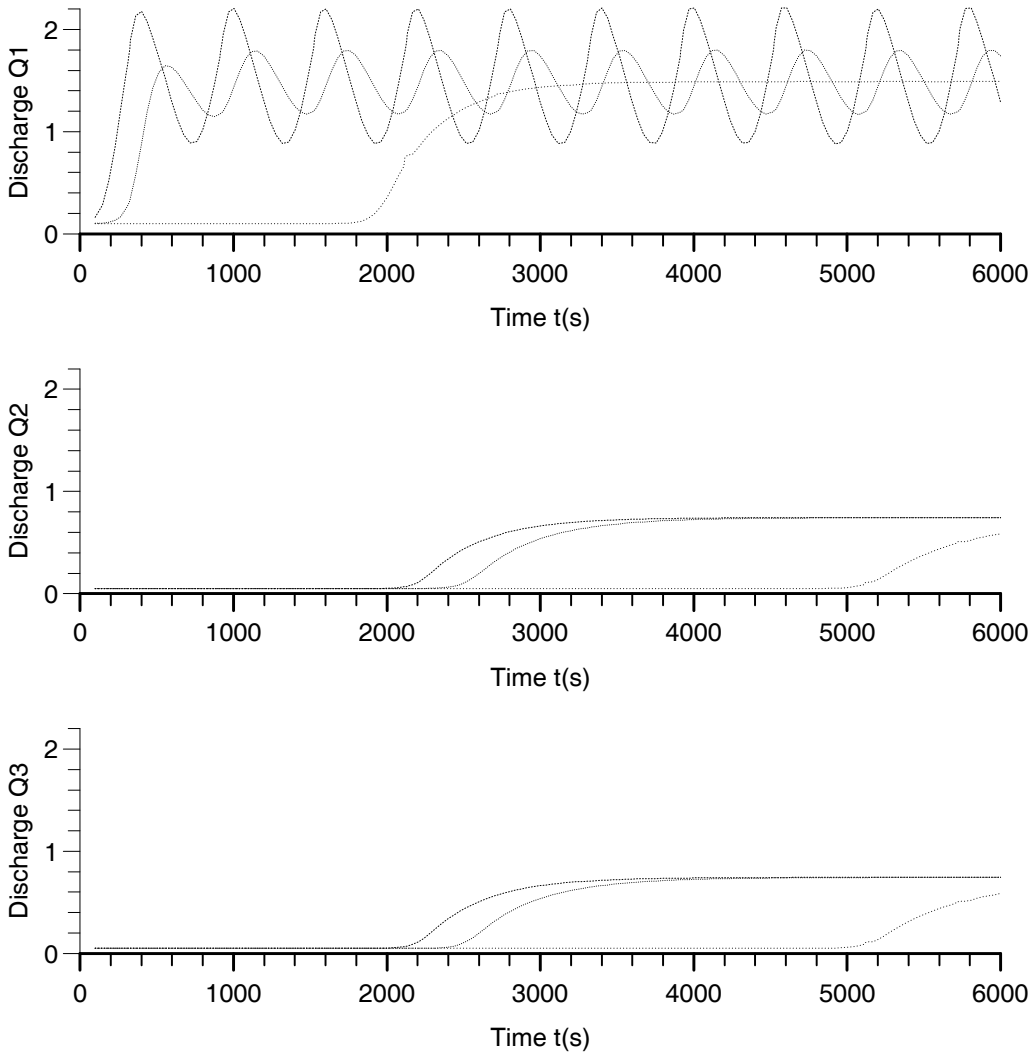

Figure 15: Discharge hydrographs. Peak value of the inflow wave $Q_M = 2.8m^3/s$. CFL=4. $\Delta x = 50m$. N= 100.

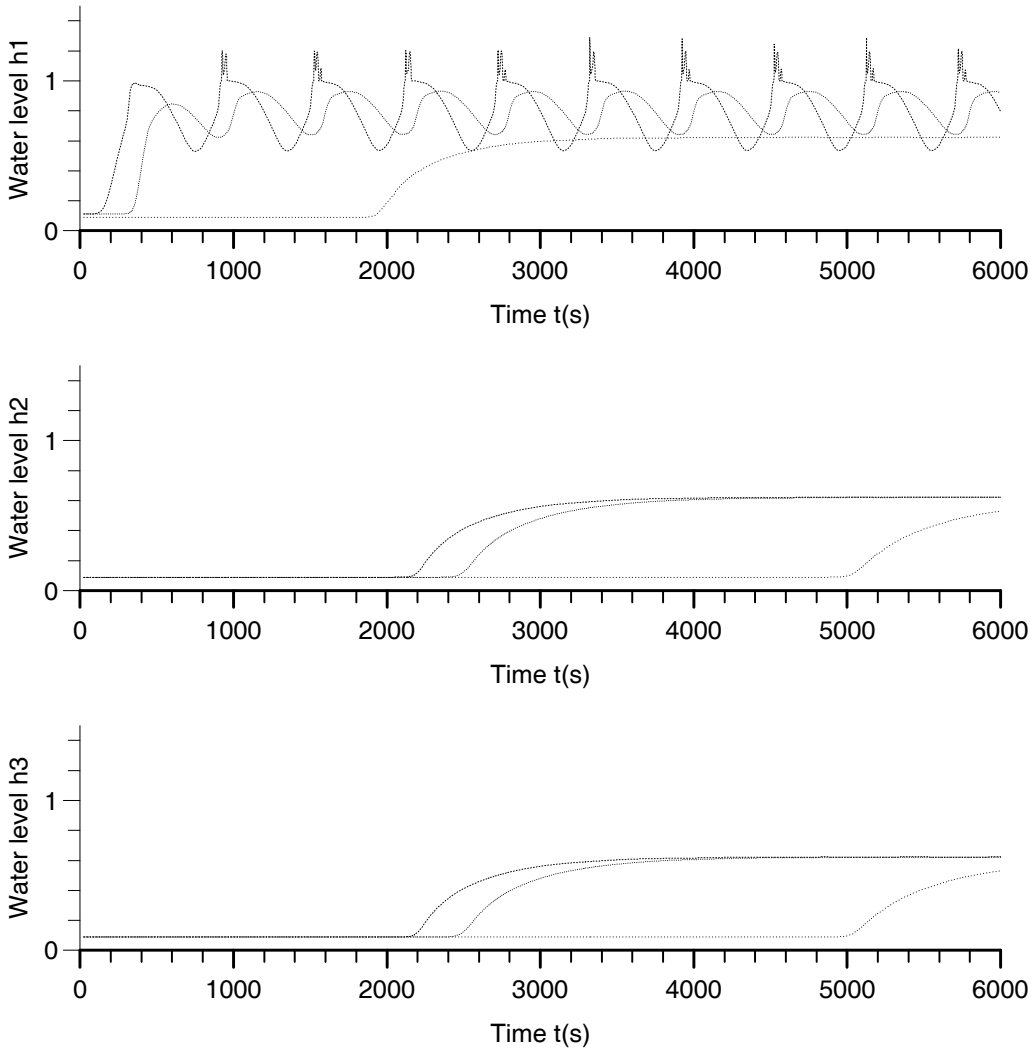

Figure 16: Water level limnigrams at different locations. Peak value of the inflow wave $Q_M = 3.2m^3/s$. CFL=1. $\Delta x = 50m$. N= 100.

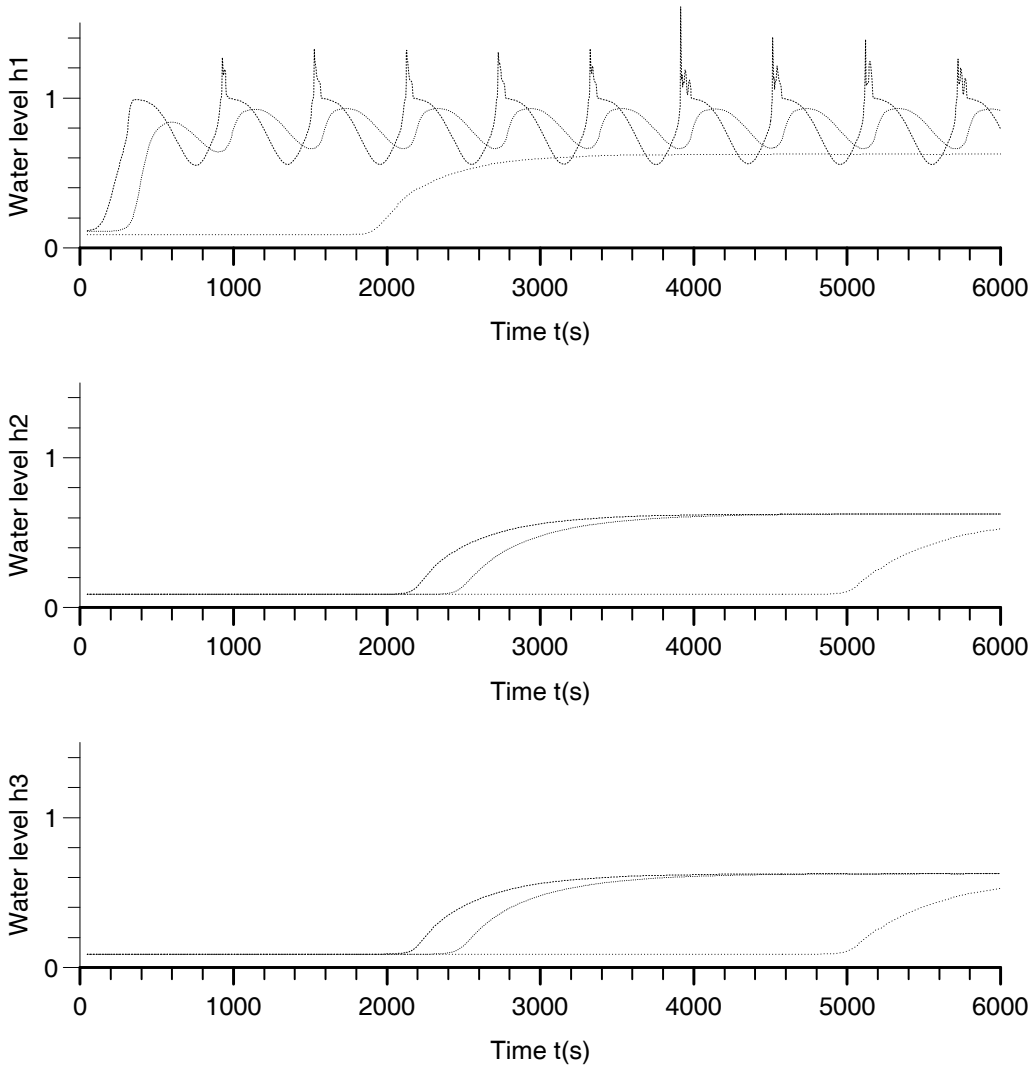

Figure 17: Water level limnigrams at different locations. Peak value of the inflow wave $Q_M = 3.2m^3/s$. CFL=2. $\Delta x = 50m$. N= 100.

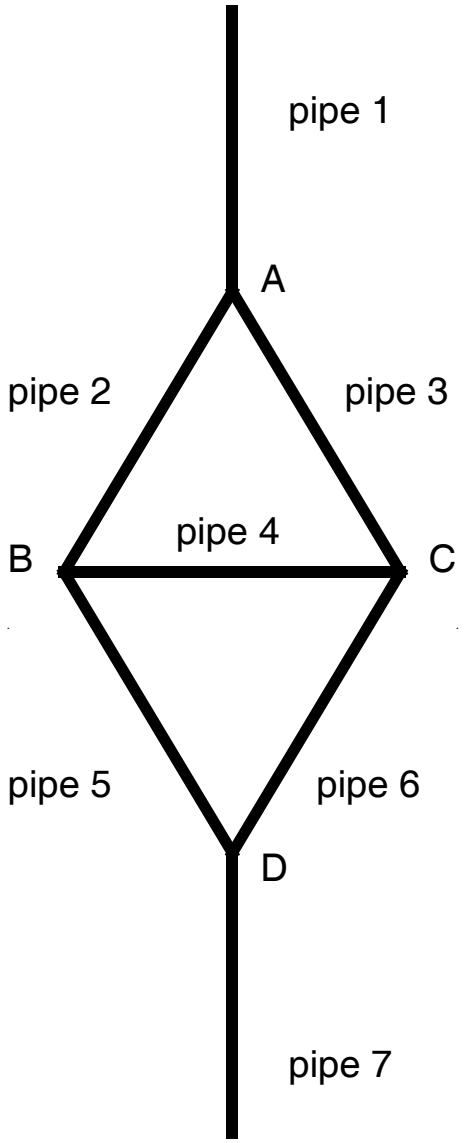

Figure 18: Looped network.

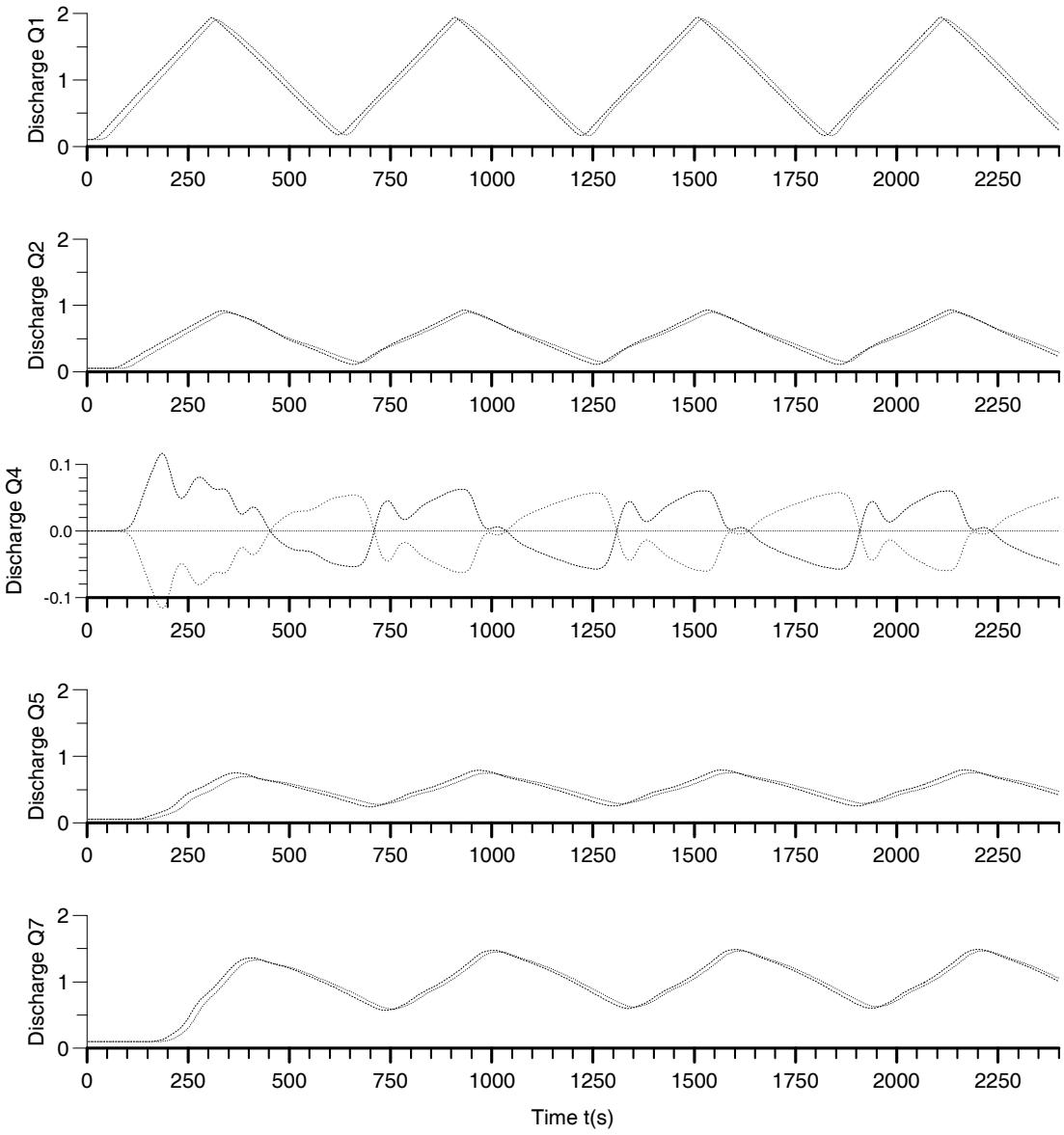

Figure 19: Looped network. Discharge history at different locations. $Q_M = 2m^3/s$. CFL=0.95. $\Delta x = 10m$. N= 10.

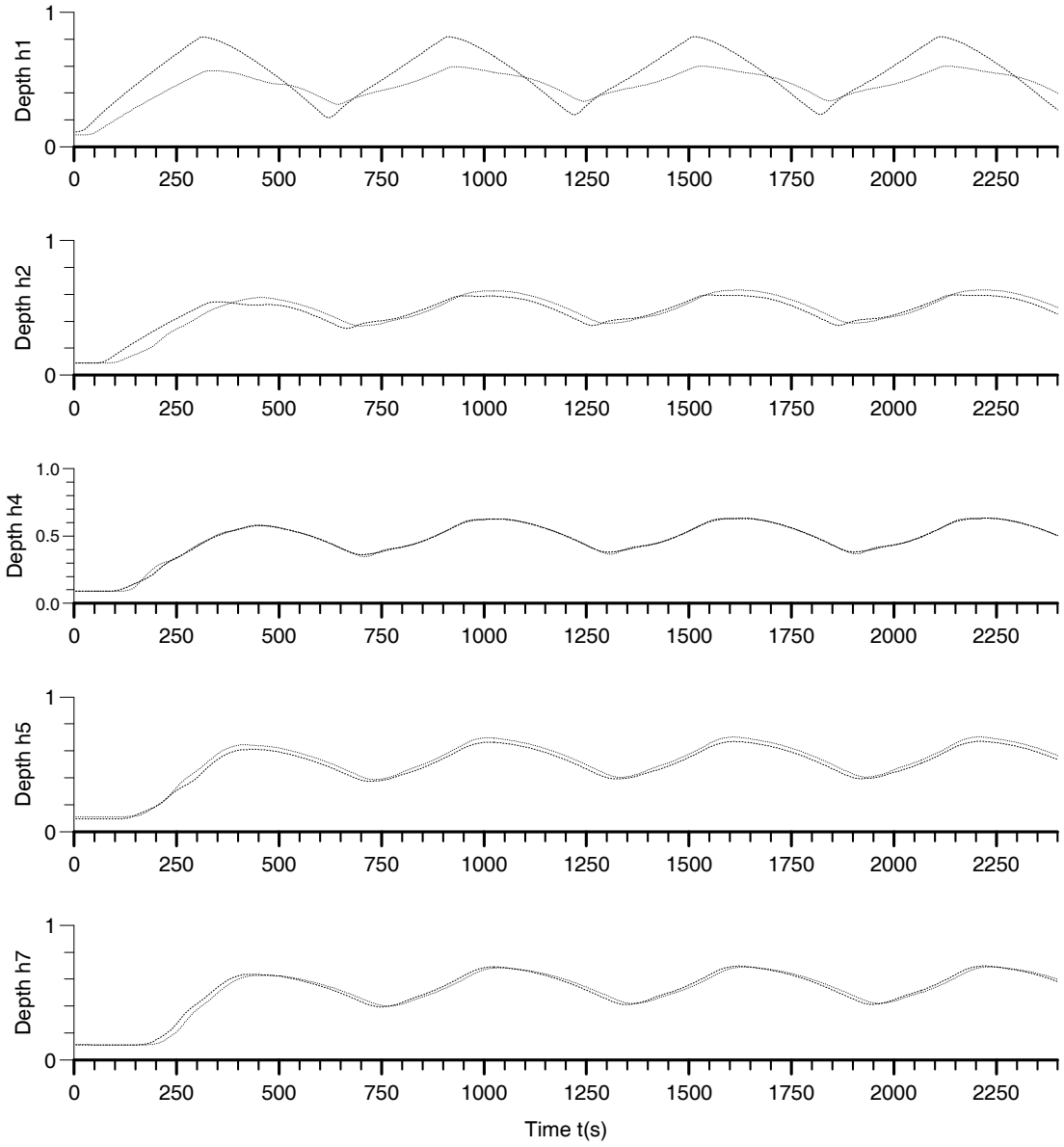

Figure 20: Depth history at different locations. Peak value of the inflow wave $Q_M = 2m^3/s$. CFL=0.95. $\Delta x = 10m$. N= 10.

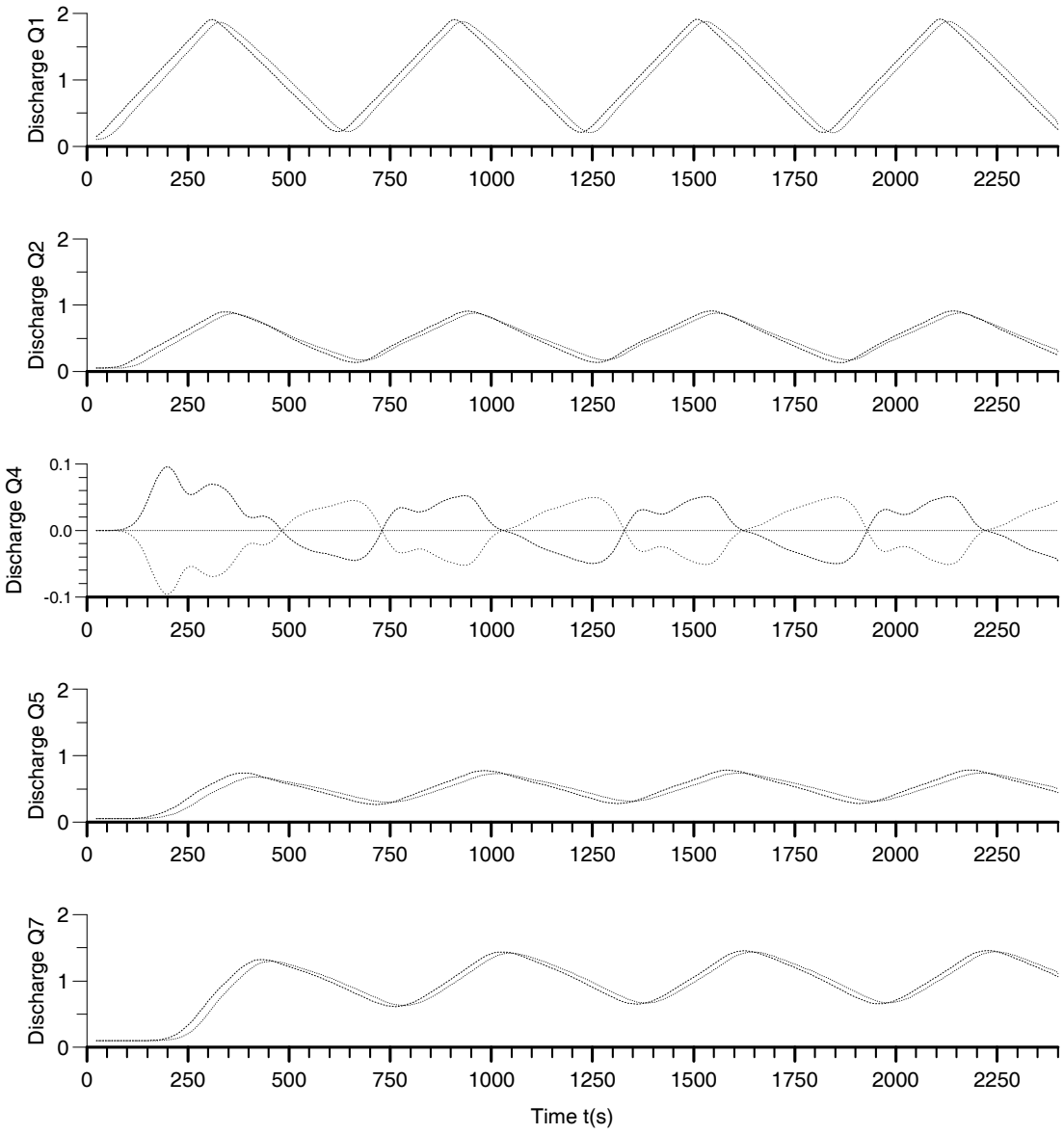

Figure 21: Discharge history at different locations. Peak value of the inflow wave $Q_M = 2m^3/s$. CFL=5. $\Delta x = 10m$. N= 10.

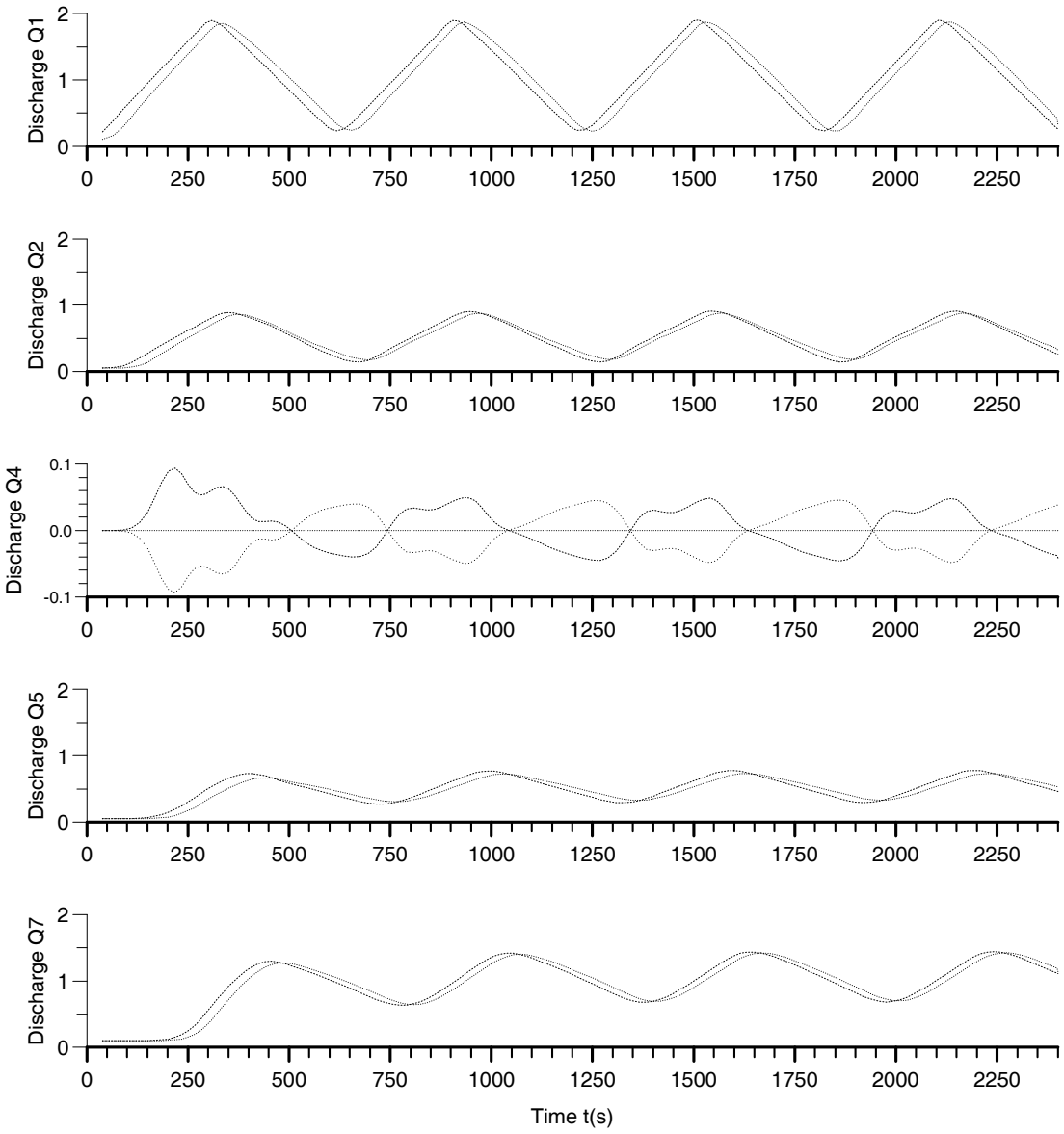

Figure 22: Discharge history at different locations. Peak value of the inflow wave $Q_M = 2m^3/s$. CFL=8. $\Delta x = 10m$. N= 10.

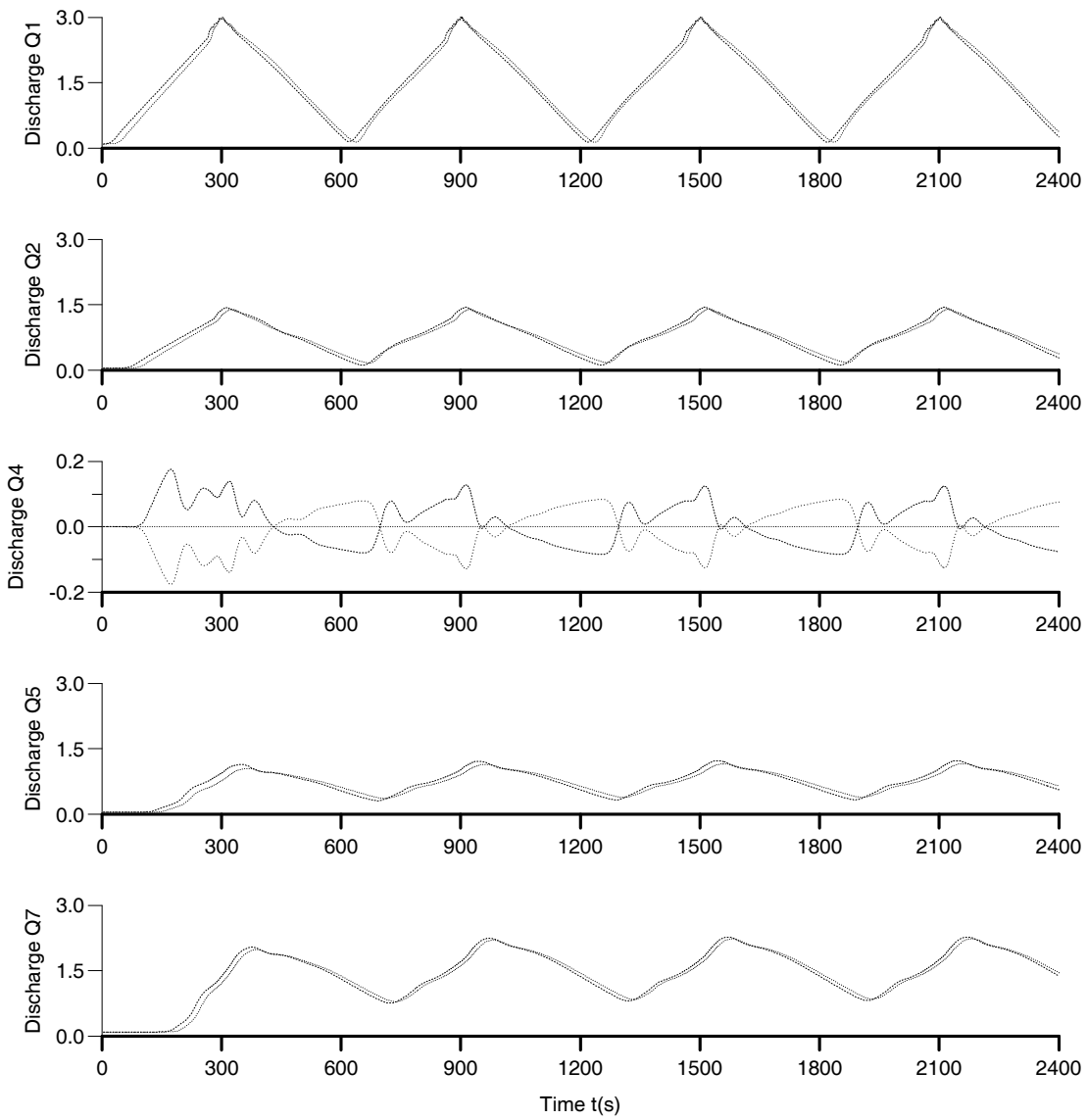

Figure 23: Discharge history at different locations. Peak value of the inflow wave $Q_M = 3m^3/s$. CFL=0.95. $\Delta x = 10m$. N= 10.

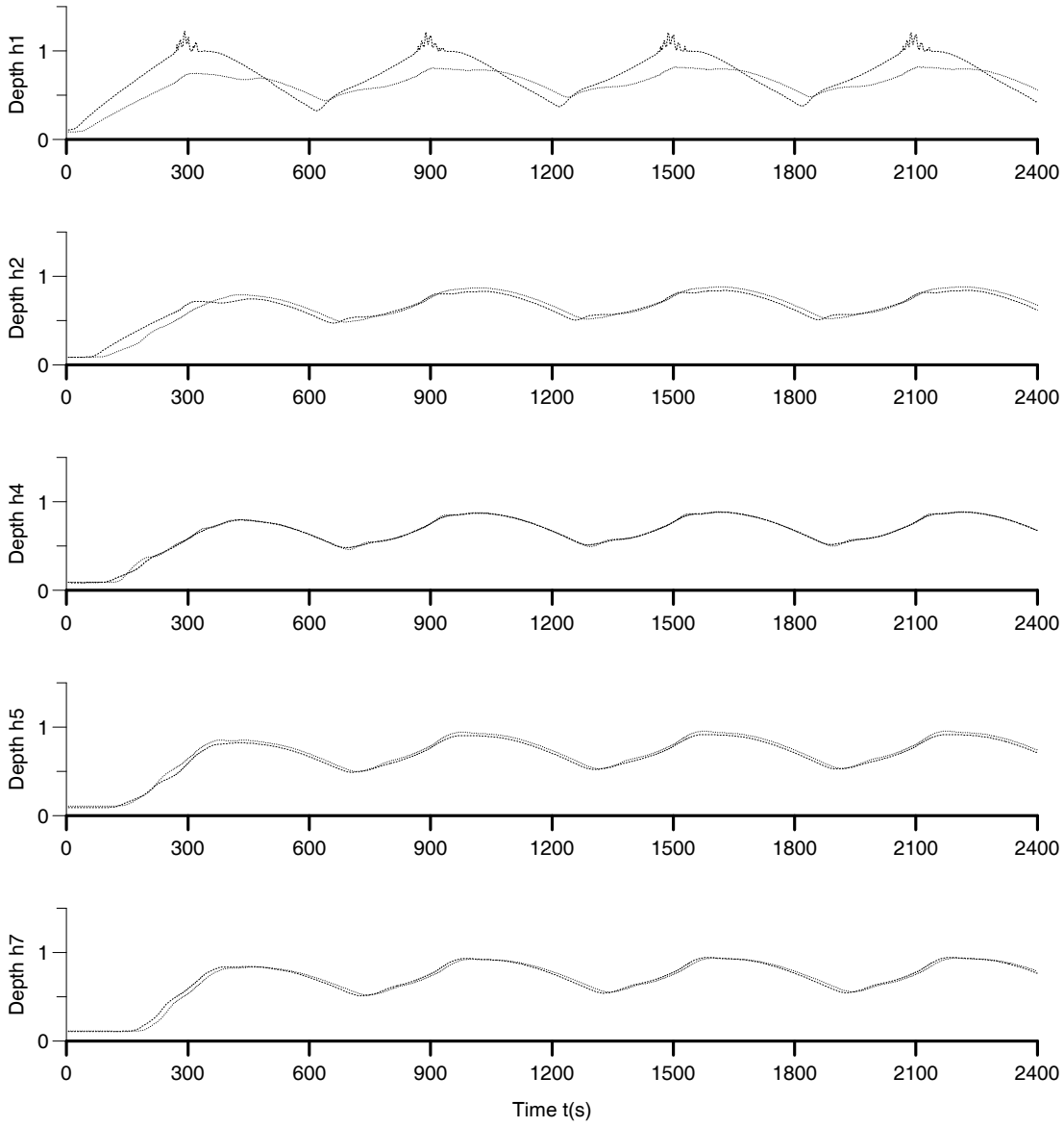

Figure 24: Depth history at different locations. Peak value of the inflow wave $Q_M = 3m^3/s$. CFL=0.95. $\Delta x = 10m$. N= 10.

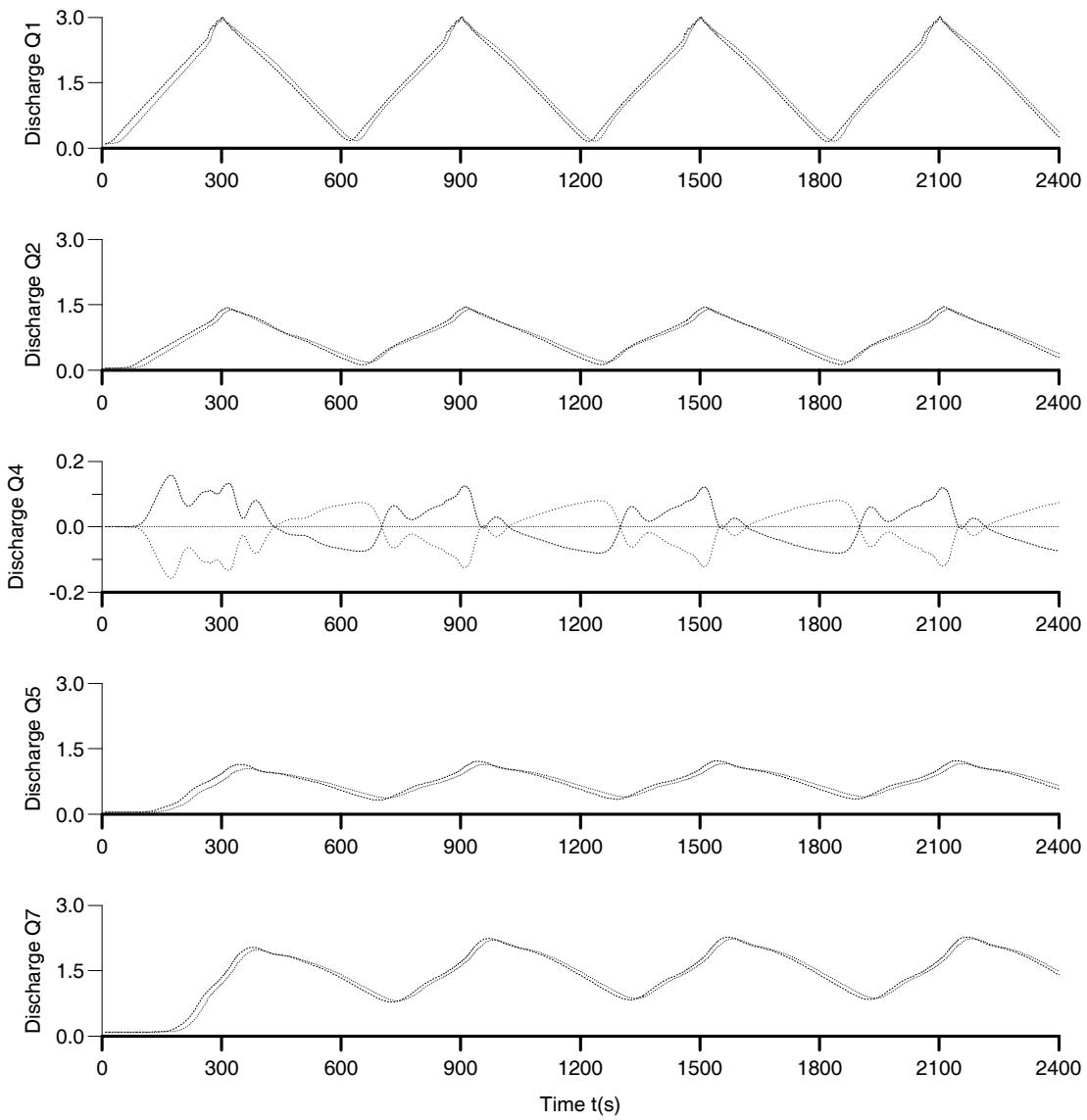

Figure 25: Discharge history at different locations. Peak value of the inflow wave $Q_M = 3m^3/s$. CFL=2. $\Delta x = 10m$. N= 10.

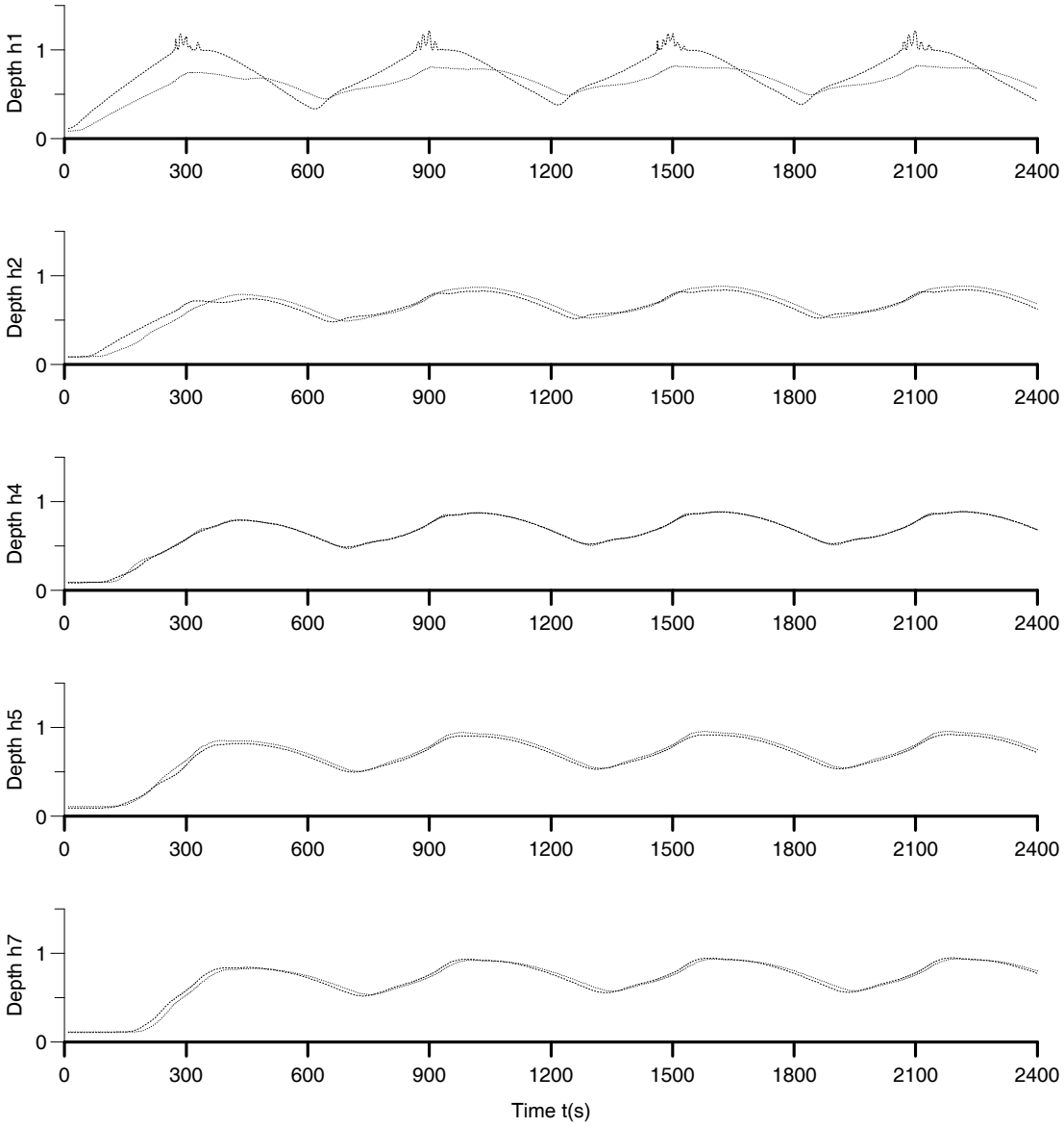

Figure 26: Depth history at different locations. Peak value of the inflow wave $Q_M = 3m^3/s$. CFL=2. $\Delta x = 10m$. N= 10.

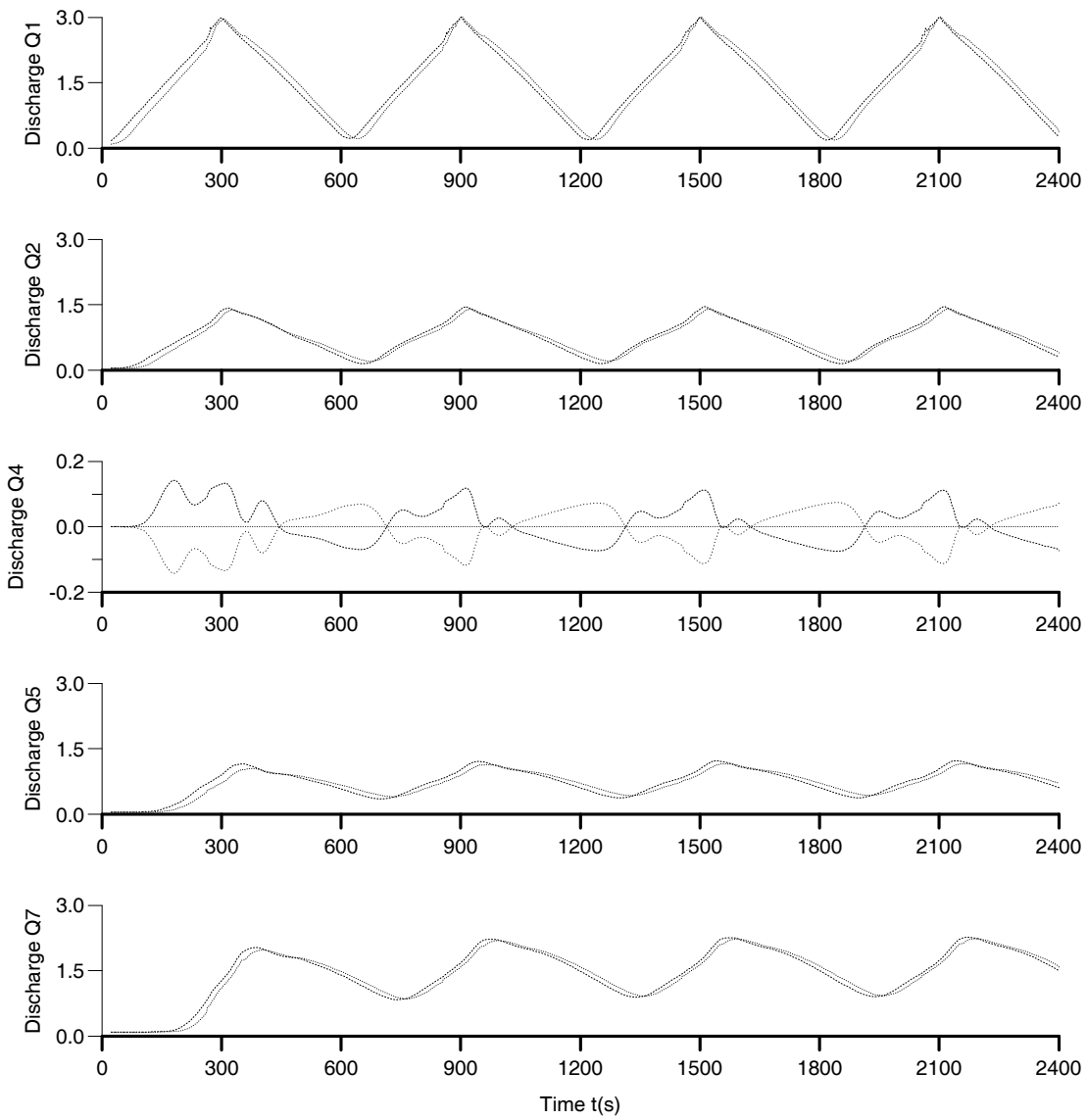

Figure 27: Discharge history at different locations. Peak value of the inflow wave $Q_M = 3m^3/s$. CFL=5. $\Delta x = 10m$. N= 10.

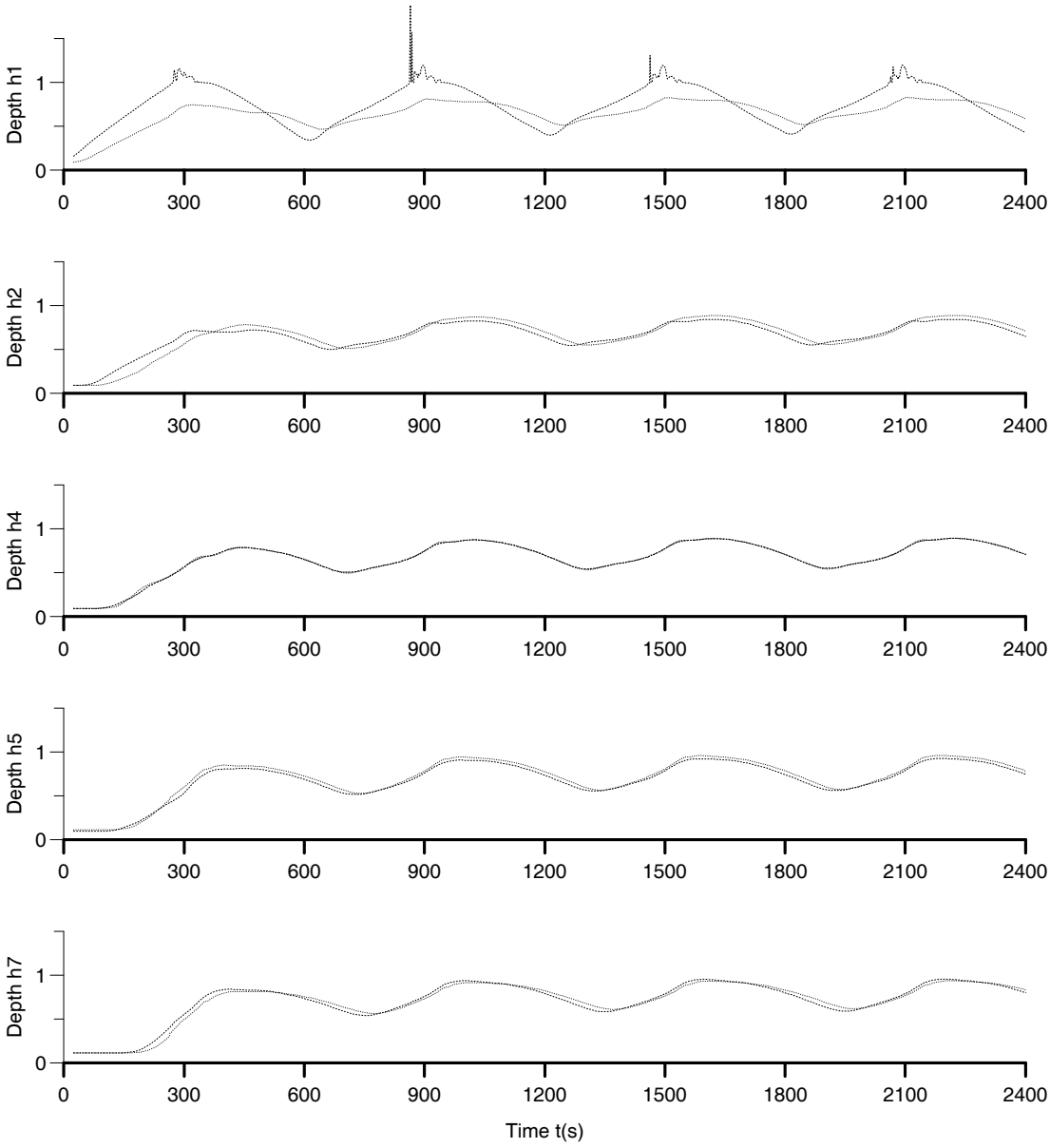

Figure 28: Depth history at different locations. Peak value of the inflow wave $Q_M = 3m^3/s$. CFL=5. $\Delta x = 10m$. N= 10.

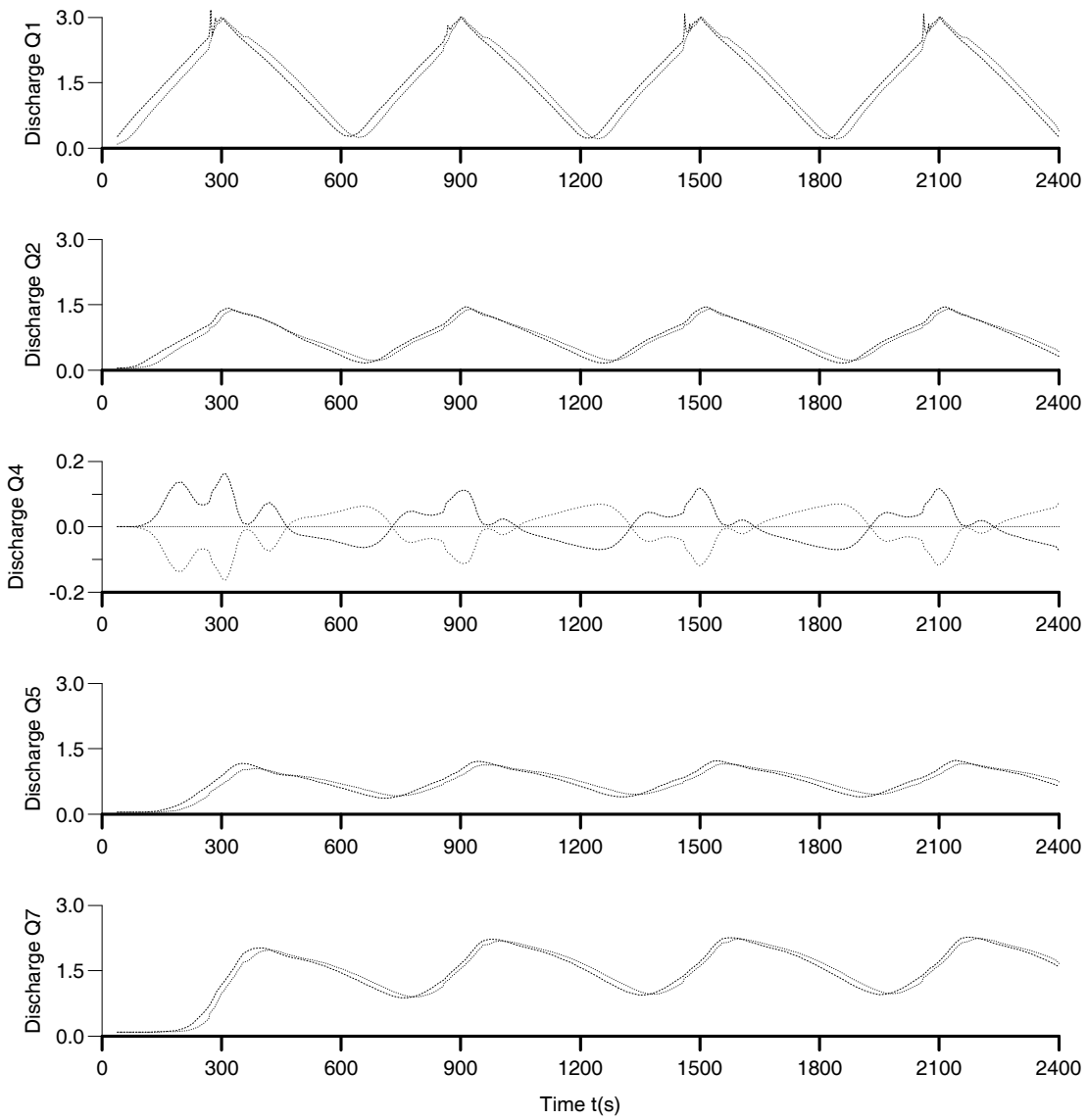

Figure 29: Discharge history at different locations. Peak value of the inflow wave $Q_M = 3m^3/s$. CFL=8. $\Delta x = 10m$. N= 10.

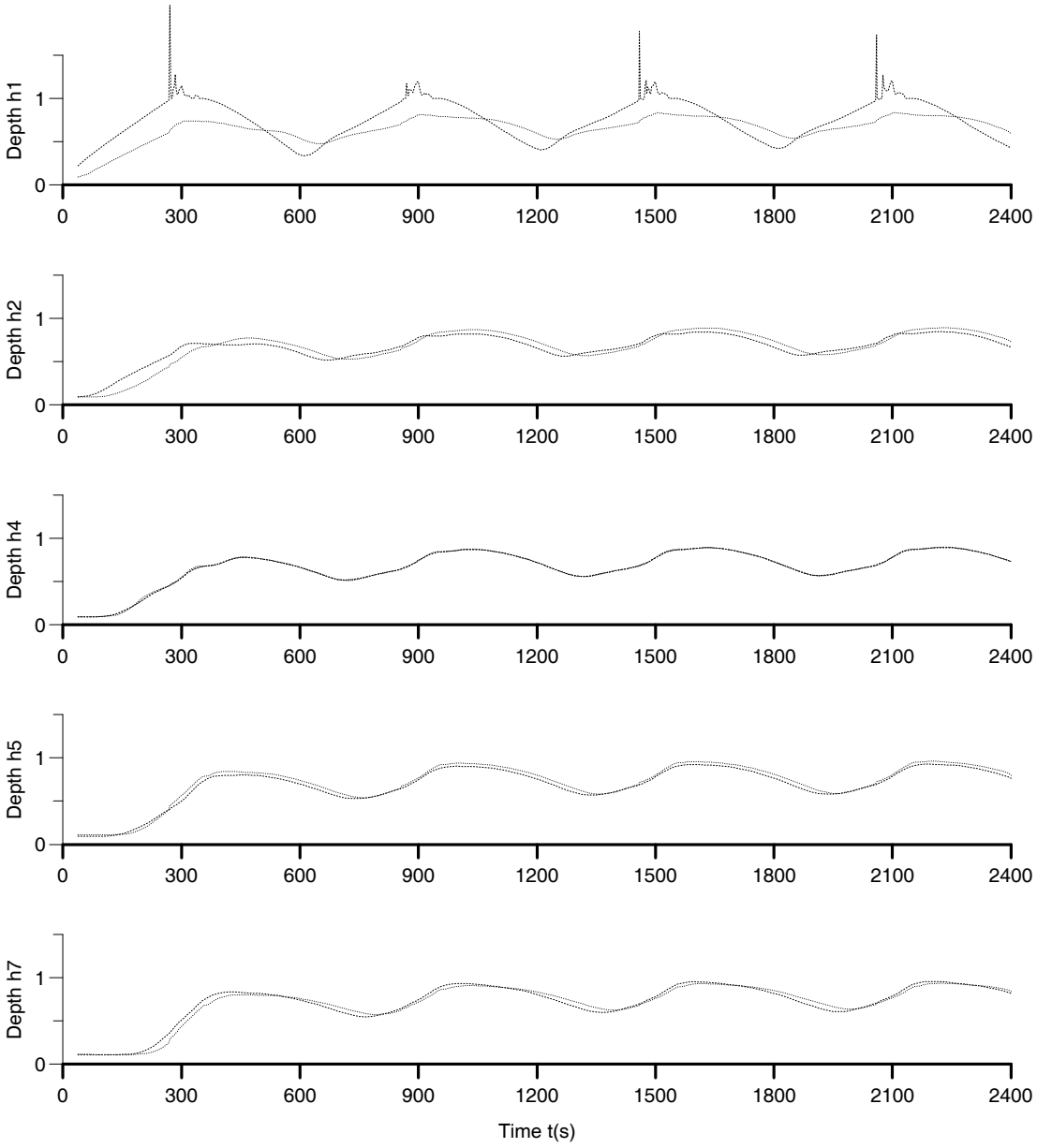

Figure 30: Depth history at different locations. Peak value of the inflow wave $Q_M = 3m^3/s$. CFL=8. $\Delta x = 10m$. N= 10.